Nuclear Physics **A485** (1988) 327-359
North-Holland, Amsterdam

QUADRUPOLE COLLECTIVE PROPERTIES OF ^{114}Cd

C. FAHLANDER

The Svedberg Laboratory, Uppsala University, S-75121 Uppsala, Sweden

A. BÄCKLIN, L. HASSELGREN, A. KAVKA, V. MITTAL[a],
L. E. SVENSSON and B. VARNESTIG

Institute of Radiation Sciences, Uppsala University, S-75121 Uppsala, Sweden

D. CLINE and B. KOTLINSKI

Nuclear Structure Research Laboratory, University of Rochester, Rochester, New York 14627, USA

H. GREIN, E. GROSSE, R. KULESSA[b], C. MICHEL[c], W. SPRENG and H.J. WOLLERSHEIM

Gesellschaft fur Schwerionenforschung, D-6100 Darmstadt, Germany

J. STACHEL[d]

Institut fur Kernchemie, Universität Mainz, D-6500 Mainz, Germany

Received 17 July 1987
(Revised 21 April 1988)

Abstract: The nucleus ^{114}Cd has been Coulomb excited using beams of ^{16}O, ^{40}Ca, ^{58}Ni and ^{208}Pb. Several new states have been observed and an almost complete set of reduced E2 matrix elements for the lowest-lying positive-parity states in ^{114}Cd have been measured. In total, about 40 E2 matrix elements have been determined in a model-independent way, including the static quadrupole moments of the 4_1^+, 6_1^+, 2_2^+ and 2_3^+ states. Large negative static quadrupole moments were found for the 4_1^+ and 6_1^+ states and a large positive quadrupole moment for the 2_2^+ state. All E2 matrix elements involved in the deexcitation of the quintuplet of states at an energy of about 1.2 MeV were determined. The data are compared with predictions by various models, including a configuration mixing calculation within the framework of the IBA model, the harmonic vibrator and a model in which the states of a near-harmonic vibrator are mixed with those of a rotational intruder band with a large deformation. Although no perfect match is obtained, the data favour a vibration-like structure involving levels up to the four-quadrupole phonon multiplet.

E

NUCLEAR REACTIONS ^{114}Cd(^{16}O, ^{16}O), $E = 45$ MeV; ^{114}Cd(^{40}Ca, ^{40}Ca), $E = 122$ MeV; ^{114}Cd(^{58}Ni, ^{58}Ni), $E = 184$ MeV; ^{114}Cd(^{208}Pb, ^{208}Pb), $E = 916$ MeV; measured pp$\gamma(\theta)$ following Coulomb excitation. ^{114}Cd levels deduced B(E2), quadrupole moment. Enriched targets.

1. Introduction

Even-even nuclei in the Ru-Te region show, in their lowest excited states, spectra typical of slightly anharmonic quadrupole vibrators, i.e. a 0^+, 2^+ and 4^+ triplet of

Present addresses:
[a] Dept. of Physics, Panjab University, Chandigarh-160014, India.
[b] Physics Dept., Jagiellonian Univ., Cracow, Poland.
[c] Univ. Catholique, Louvain-la-Neuve, Belgium.
[d] State University of New York, Stony Brook, New York 11794, USA.

states occurs at about twice the energy of that of the first excited 2^+ state. The experimental $B(E2)$ values for some of the transitions between these low-lying levels also agree rather well with the predictions of the vibrator model. However, the energy spectra are often complicated by additional "intruding" states and more recent experiments and theoretical calculations indicate that different types of deformation and even coexistence of deformations may occur.

The best example of coexisting shapes is found in the Sn ($Z = 50$) isotopes. For these nuclei low-lying deformed 0^+ intruder states with an associated rotational band structure have been found [1,2]). Experimental evidence of similar 0^+ rotational bands also exists in the neighbouring Te ($Z = 52$) nuclei [3]). The deformation has been suggested to originate from two-particle two-hole (2p2h) excitations in the $Z = 50$ closed proton shell. Studies of the E0 and E2 transition probabilities, depopulating the low-lying low-spin states in $^{112-124}$Sn [refs. [1,4,5])], indicate strong admixtures between the intruder states and the states with a vibrational 2-phonon character.

The most sensitive measures of the collectivity of nuclei are their electric quadrupole degrees of freedom, which preferably are studied using Coulomb excitation. Two such experiments, utilising the most recent advances in Coulomb excitation, have been performed in this region on ^{104}Ru ($Z = 44$) [6-8]) and ^{110}Pd ($Z = 46$) [9]). It was found that the ground state of ^{104}Ru has a triaxial deformation, and that the 0^+ state in the triplet very likely is based on an intruder configuration somewhat less deformed than the ground state. In ^{110}Pd 110 diagonal and transitional E2 matrix elements were determined. From them it was concluded that all low-lying states can be grouped in four bands of predominantly rotational structure.

In the even-even $^{110-114}$Cd ($Z = 48$) nuclei, intruding 0^+ and 2^+ states occur close to the 2-phonon triplet, producing a quintuplet of levels rather than a triplet. The collective origin of the quintuplet has been subject to many speculations, but the available data so far are insufficient to draw any definite conclusions regarding its origin (see e.g. Julin *et al.* [10]) and Heyde *et al.* [11])).

We present here an investigation of ^{114}Cd by means of Coulomb excitation with the aim to provide an experimental basis large enough to make possible a detailed comparison with various collective model predictions.

2. Experimental method

The nucleus ^{114}Cd was Coulomb excited using ^{16}O projectiles from the Uppsala EN tandem, ^{40}Ca and ^{58}Ni beams from the tandem accelerators in Rochester and Brookhaven respectively, and a ^{208}Pb beam from the UNILAC accelerator at GSI in Darmstadt. The measurements were carried out at distances between the surfaces of the two colliding nuclei exceeding 5 fm, except for the Pb experiment in the most backward direction, where the distance was 4.6 fm. There are a lot of experimental data, which show that for heavy ions, at a separation of the nuclear surfaces of

5 fm, it is safe to treat the process in terms of pure Coulomb excitation theory [12]). At 4.6 fm it is likely that the influence of nuclear interactions on the inelastic excitation is larger, particularly for the higher spin states [13]) However, compared to other sources of error in the ^{208}Pb experiment, the influence from Coulomb-nuclear interference at 4.6 fm is expected to be small, and thus all data were analysed assuming pure electromagnetic interaction.

In the ^{16}O experiment the energy of the beam was 45 MeV, and it was stopped in a thick ^{114}Cd target enriched to 98.55%. The target chamber was placed inside a large (24.5 cm outer and 8.5 cm inner diameter by 30.5 cm long) annular NaI detector. A Ge(Li) detector, at a distance of only 9 mm from the target and at an angle of 0° with respect to the beam, was also placed inside the annulus. The Ge(Li) and the NaI detectors were operated in coincidence with each other. Due to the large solid angle of the NaI annulus, and the close geometry, the two detectors comprise a high efficiency $\gamma\gamma$-coincidence system. A gate was set on the $2_1^+ \rightarrow 0_1^+$ transition in the NaI spectrum to project the Ge(Li) spectrum. This increases considerably the sensitivity for some of the low intensity γ-rays in the Ge(Li) detector as compared to a singles experiment. A detailed description of this high efficiency setup is given by Jonsson *et al.* [14]). The γ-ray yields were corrected for angular correlation and solid angle effects. The relative efficiency of the Ge(Li) detector was obtained using standard radioactive γ-ray sources. A typical $\gamma\gamma$-coincidence spectrum is shown in fig. 1.

The ^{40}Ca and ^{58}Ni experiments were performed at energies of 122 and 184 MeV respectively. In both of these experiments self-supporting, about 0.35 mg/cm^2 thick, enriched (98.55%) targets, were used. The deexciting γ-rays were detected in two and four Ge(Li) detectors respectively. In the Ca experiment they were placed at angles of +25° and −25°, and in the Ni experiment at +18°, +155°, −18° and −155° with respect to the beam direction. The Ge(Li) detectors were operated in triple coincidence with the scattered projectiles and recoiling nuclei, which were detected in 4 position-sensitive parallel plate avalanche gas detectors. They were placed symmetrically around the beam axis and covered, in the Ca experiment, a polar angular range in the laboratory frame of $12° < \theta < 72°$ and $104° < \theta < 144°$ with an azimuthal angle, ϕ, between −25° and +25°. In the Ni experiment the ranges were $8° < \theta < 76°$ and $104° < \theta < 152°$ and $-35° < \phi < +35°$. The geometry in the latter experiment is shown as an example in fig. 2. A description of the particle counters is given in ref. [15]).

In the GSI experiment a ^{208}Pb beam with an energy of 992 MeV was used. A Ti foil of thickness 0.94 mg/cm^2 was placed in front of the target to reduce the incident beam energy to about 916 MeV. The ^{114}Cd target was enriched to 98.55% and had a thickness of 0.35 mg/cm^2. Due to the uncertainty in the thickness of the two foils and an estimated uncertainty in the stopping power values [16]) of about 10%, the uncertainty in the beam energy was estimated to be about 2%. Triple coincidences were recorded between the scattered projectiles, the recoiling target nuclei and the

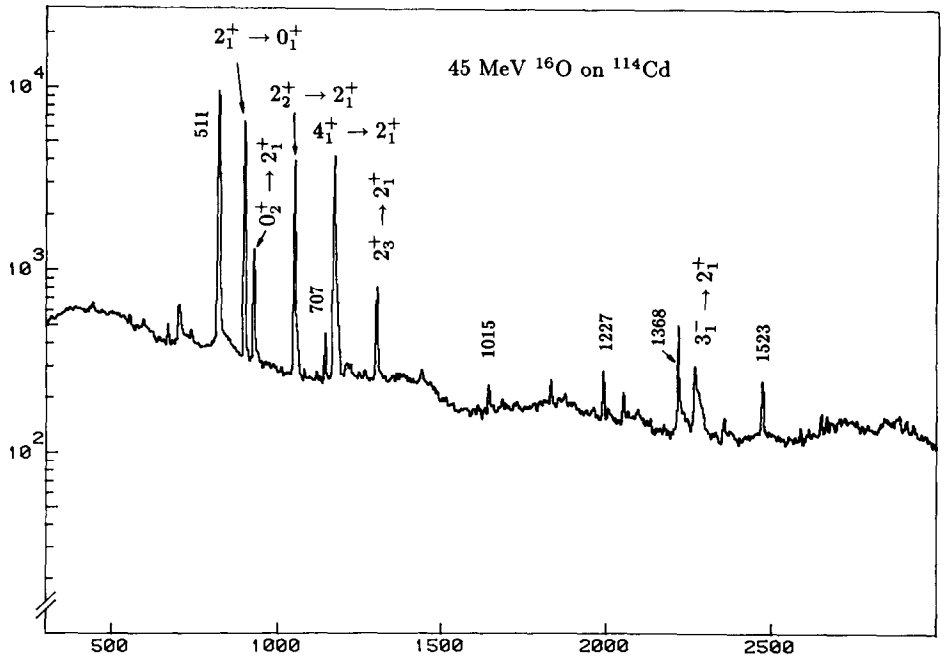

Fig. 1. A Ge spectrum gated on the $2_1^+ \rightarrow 0_1^+$ transition in the NaI spectrum, following the excitation of ^{114}Cd with 45 MeV ^{16}O projectiles. The $2_1^+ \rightarrow 0_1^+$ transition is present in the gated spectrum, because the Compton events from the higher energy transitions are in the gate as well as the $0_2^+ \rightarrow 2_1^+$ transition, which can not be resolved in the NaI spectrum. The 707, 1015 and 1368 keV impurity lines originate from the reactions ^{16}O(^{16}O, pn)^{30}P, ^{27}Al(n, n') and ^{16}O(^{12}C, α)^{24}Mg, respectively. The other two impurity lines, 1227 and 1523 keV, have not been identified.

deexcitation γ-rays. The particles were detected in two large-area position sensitive gas counters placed about 15 cm from the target, each subtending a polar angle between 17° and 58° on each side of the beam axis. The relatively large distance between the target and the particle detectors made it possible to distinguish between a Cd recoil and a Pb projectile by a time-of-flight technique using the prompt signal from the anodes of the detectors. For a Cd recoil detected in either of the two detectors the equivalent center-of-mass scattering angles of the Pb projectiles range between $64° < \theta < 146°$. The azimuthal angular range was in this case $-28° < \phi < +28°$. These detectors are described in more detail in ref. [17]). The γ-rays were detected in 3 Ge(Li) detectors placed at 30°, 150° and 210° with respect to the beam direction.

The γ-ray yields were obtained for each projectile as a function of the scattering angle by setting windows on the corresponding position spectrum. Due to the large recoil velocities of the deexciting nuclei, about $0.1c$ in the Pb experiment, the γ-ray peaks were broadened appreciably by the Doppler effect. However, the position sensitivity of the particle detectors made it possible to reconstruct the kinematics

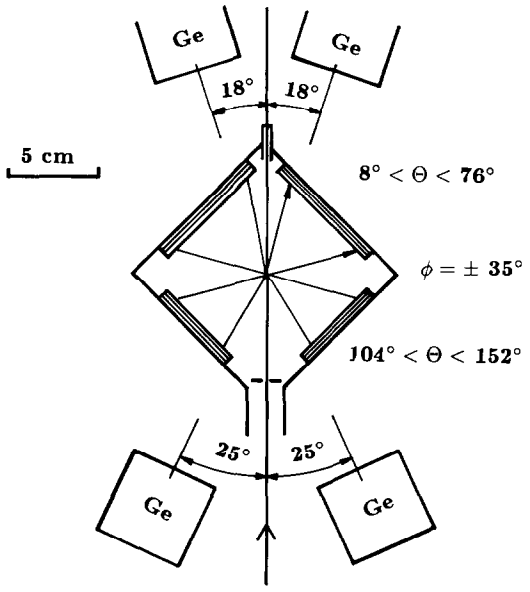

Fig. 2. The experimental set-up in the Ni experiment showing the position of the four Ge detectors and the four particle detectors.

for each scattering event and the observed γ-ray energy thus can be corrected to first order for the Doppler shift on an event-by-event basis. A Doppler-corrected γ-ray spectrum obtained in the Ni experiment is shown in fig. 3 and for the Pb experiment in fig. 4. In the latter experiment the final energy resolution was about 6 keV at 559 keV.

3. Level scheme of ^{114}Cd

The nucleus ^{114}Cd recently has been investigated in a thermal neutron capture experiment [18]). An almost complete level scheme, comprising 49 levels with spins ≤ 4 was constructed up to an energy of about 3.3 MeV. No states with spin 6 or higher were observed. The partial level scheme of fig. 5 shows all even spin, positive-parity states below an excitation energy of about 2.4 MeV. In the present Coulomb excitation experiment 11 of these states were excited. In addition three more γ-rays, not previously known, were observed. They are tentatively assigned as transitions from higher spin states.

In the ^{16}O and ^{40}Ca experiments the highest spin state excited was the 4_1^+ state, and no states above the quintuplet were observed. With the Ni beam an additional γ-ray (above the quintuplet) with an energy of about 707 keV was observed with an intensity of about 1% of the intensity of the $2_1^+ \rightarrow 0_1^+$ transition. This transition was observed relatively strongly in the Pb experiment. In the forward scattering

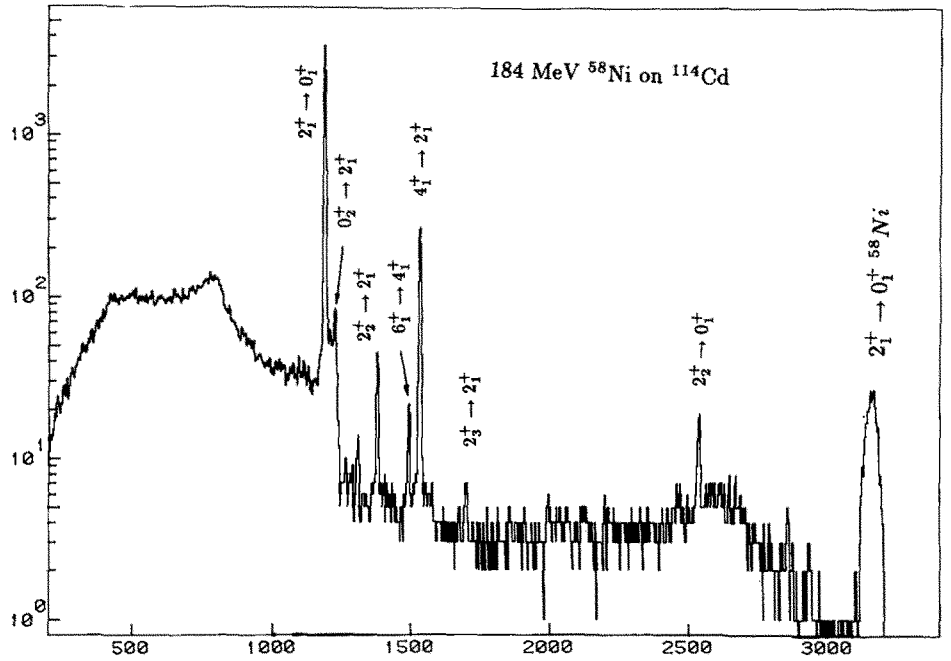

Fig. 3. A Doppler corrected γ-ray spectrum in coincidence with scattered particles following the excitation of ^{114}Cd with 184 MeV ^{58}Ni projectiles scattered about 70° in the centre-of-mass system.

direction its intensity was about 2% and in the backward direction about 6% of the $2_1^+ \to 0_1^+$ intensity. A possible explanation of this transition is that it corresponds to the transition between the 2_4^+ and 0_2^+ states. However, from the known branching ratio, $I_\gamma(2_4^+ \to 2_1^+)/I_\gamma(2_4^+ \to 0_2^+) = 1.45(15)$ [ref. [18])], and from our observed $2_4^+ \to 2_1^+$ yield, it can be concluded that only about 8% of the intensity of the 707 keV line belongs to the $2_4^+ \to 0_2^+$ transition. The main contribution is thus due to an unknown transition and it is tentatively assigned as the deexcitation of the 6_1^+ state to the 4_1^+ state. This assignment is supported by the expected Coulomb excitation yield and its angular distribution, by the energy systematics of the $6_1^+ \to 4_1^+$ transitions in the neighbouring Cd isotopes and by the fact that all 0^+, 2^+ and 4^+ states are known in this energy region [18]).

In the ^{208}Pb experiment the 4_2^+, 4_5^+, 2_4^+ and 2_5^+ states were populated weakly, the last two states being about 4 times weaker than the first two states. These states were clearly observed by summing the γ-spectra for the first 5 position windows and for the 5 last. Their intensities range between 0.5% and 2% of the $2_1^+ \to 0_1^+$ intensity. The known 4_3^+ and 4_4^+ states were not observed. In addition two more unknown transitions with energies of 668 and 679 keV were observed. They are tentatively assigned as decaying from a possible second 6^+ state and a possible first 8^+ state. The calculated yields of the $6_2^+ \to 4_2^+$ and $8_1^+ \to 6_1^+$ transitions, using E2 matrix elements for the two transitions estimated from the simple rotational and vibrational

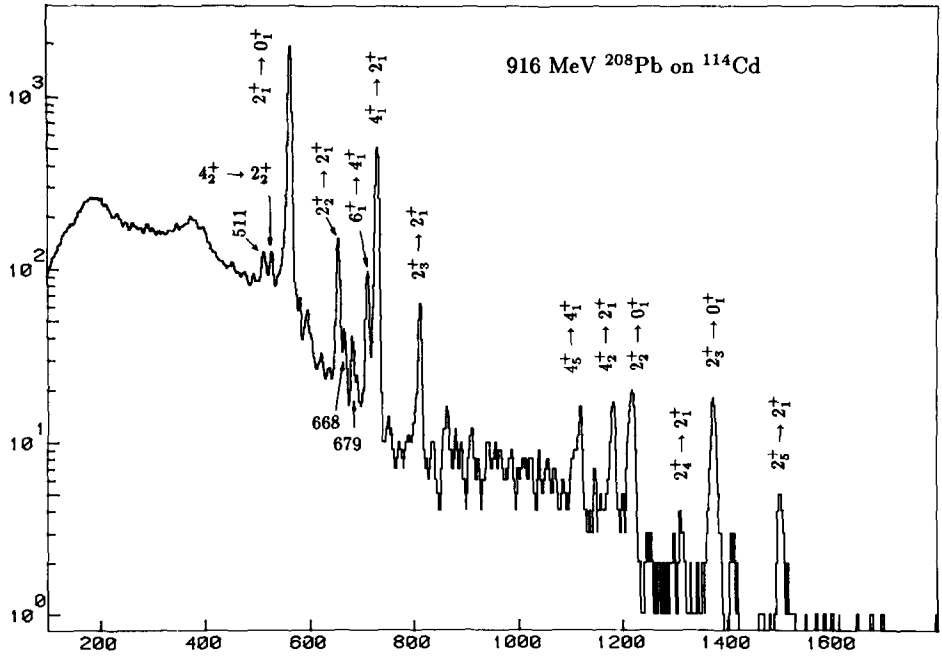

Fig. 4. A Doppler corrected γ-ray spectrum in coincidence with scattered particles following the excitation of ^{114}Cd with 916 MeV ^{208}Pb projectiles scattered about 90° in the centre-of mass system.

models respectively, suggest they should be seen in the Pb experiment, with rather similar intensities. This is in support of the assignment, but it is not possible to draw any conclusion as to which of the two energies belong to which transition.

4. Analysis

The population of the levels in Coulomb excitation is dominated by the E2 transitions and the corresponding E2 matrix elements are determined by measuring the Coulomb excitation cross sections. In the present study the cross sections are obtained from the observed deexcitation γ-ray yields, measured as a function of the scattering angle for each projectile.

The diagonal and off-diagonal reduced E2 matrix elements $\langle I_s \| M(E2) \| I_r \rangle$ are defined by:

$$\langle I_s M_s | M(\mathrm{E2}, \mu) | I_r M_r \rangle = (-1)^{I_s - M_s} \begin{pmatrix} I_s & 2 & I_r \\ -M_s & \mu & M_r \end{pmatrix} \langle I_s \| M(\mathrm{E2}) \| I_r \rangle ,$$

where $M(\mathrm{E2})$ is the electric quadrupole operator. In addition to the E2 matrix elements, the M1 admixture of the transitions must be considered for the deexcitation. These matrix elements are defined similarly. The number of unknown matrix

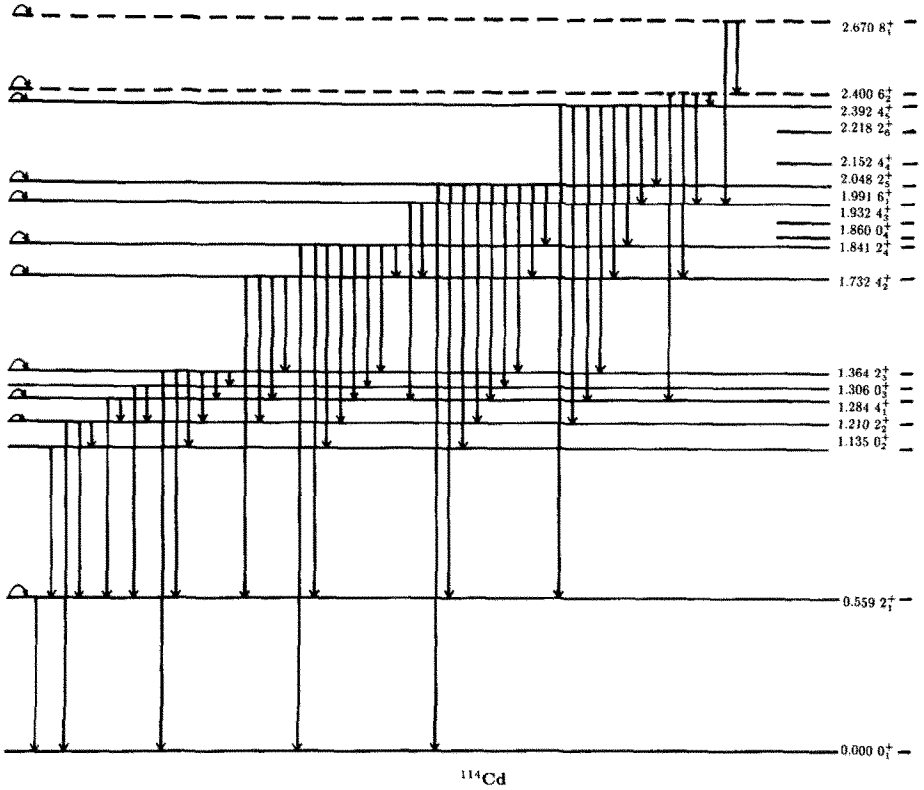

Fig. 5. A partial level scheme of ^{114}Cd showing all known levels [18]) below about 2.4 MeV of excitation energy. Also two 6^+ states and one 8^+ state, suggested in the present experiment are shown. All these levels were included in the analysis. The states observed in the present experiment are indicated with a wider horizontal bar. The arrows indicate all 63 possible E2 matrix elements to the observed levels.

elements included in the present analysis is 86. In the ^{16}O bombardment only a small number of them will participate in the excitation process, whereas for a heavy projectile like Pb, this number increases dramatically, making the analysis of the data more difficult. However, due to the variation of the strength of the interaction, through the projectile Z-values and through the scattering angles, it is possible to successively determine more and more matrix elements.

The Coulomb excitation cross sections are sensitive to the relative signs as well as the magnitudes of the matrix elements. The phase of each level wave function is fixed by arbitrarily choosing the signs of the E2 matrix elements according to the encircled signs of fig. 6. This can be done without any loss of generality. The remaining signs are determined relative to the fixed signs, and are, in principle, physical observables. The signs of the diagonal matrix elements are independent of the phase chosen for the wave function and in several cases were determined unambiguously.

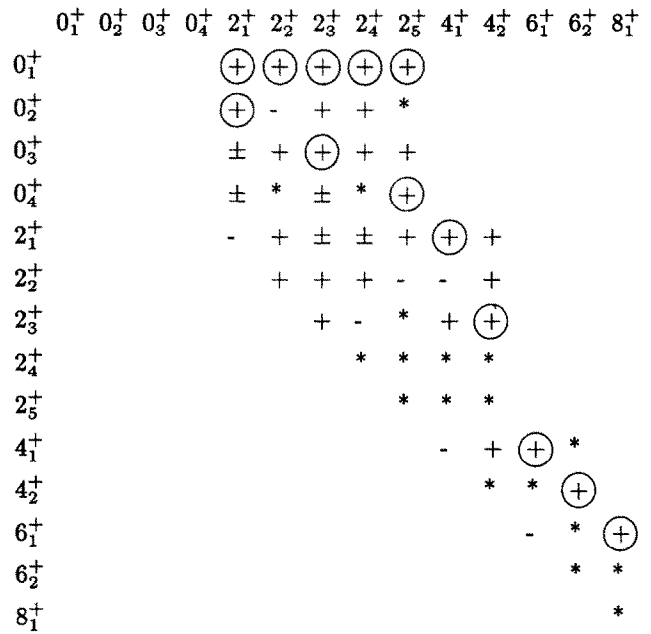

Fig. 6. The signs of the E2 matrix elements determined in the present experiment. A ± sign means that the sign of the matrix element could not be determined and an asterisk means that the matrix element was not determined. The encircled signs have been chosen arbitrarily to fix the signs of the wavefunctions of the states.

4.1. THE CODE GOSIA

The data were analysed using the newly developed coupled-channels, least-squares search routine, GOSIA [19]). GOSIA treats the Coulomb excitation process semiclassically. It can handle up to 50 energy levels and make a least-squares fit of up to 200 matrix elements, of different Eλ and Mλ multipolarities, to 50 independent sets of Coulomb excitation data. The Coulomb excitation yields are initially calculated for a set of random matrix elements. The matrix elements are then varied according to a steepest descent minimization, and at each step of minimization the result is compared with experiment. This iterative procedure is repeated until a minimum is reached, the goodness of which is determined by the normal χ^2 criterion. Due to the large energy level system and the vast amount of data included, the calculations may become very time consuming. Fast analytical approximations are used to speed up the calculations by several orders of magnitude.

4.2. EXPERIMENTAL INPUT

The total number of levels excited in the present experiments is 13. However, there may be more states that influence the excitation probabilities of the observed

states through real or virtual excitations. The final analysis therefore includes the additional unobserved levels below about 2.4 MeV shown in fig. 5. Neither the negative-parity states, nor the 3_1^+ states were included. The effect of including them is discussed in the following subsections. Also included were the 10_1^+, 8_2^+ and 6_3^+ states for which the energies and $B(E2)$ values were estimated using the rigid rotor model and results from the IBA-2 calculations. The final analysis thus comprises 21 levels. A total of 86 matrix elements are included, which accounts for most M1 and E2 couplings between the 21 levels. The 63 diagonal and off-diagonal E2 couplings to the 14 observed states are shown in fig. 5.

The oxygen experiment only represents one interval of scattering angles, but for the Ca, Ni and Pb experiments 5, 12 and 10 different windows were set on the respective position spectra, where each window covers an angular range of about 10° to 15°. The precision of the scattering angles are measured to about 0.5°. In the Ca and Ni experiments, not the full angular range of the particle detectors was used, since in the most forward angles the excitation probabilities are very small. Thus e.g. in the Ni experiment the most forward gate was set between 42° and 53°. An uncertainty of 0.5° in the scattering angle produces an uncertainty of the integrated excitation probability of the 6_1^+ state of about 4% and less for the lower-lying states. In addition, in the Pb experiment, the 5 first and the 5 last windows were summed together in order to observe the weakly populated states. In total, 30 experimental sets of γ-ray yields were measured.

There are only 16 γ-ray transitions observed, for which 492 experimental yields were measured. In the oxygen experiment no γ-yields were measured to better than 15%. The accuracies in the other experiments range between 6% for the most intense lines and up to 50% for the weaker lines. They were included in the analysis together with 25 branching ratios, 4 mixing ratios and one lifetime previously known from other experiments, i.e. in total 522 experimental data points. The half-life of the 0_3^+ state was known from two different experiments [10,20]) with identical results, $T_{1/2} = 5.5 \pm 0.3$ ns. The branching and mixing ratios taken from the literature are listed in table 1.

The experimental data are sensitive only to about 40 of the 86 matrix elements included, which thus are fitted to the 522 experimental data points. A sample of the experimental γ-ray yields together with the calculated yields obtained with the best fit is shown in figs. 7 and 8. The matrix elements resulting from the fit are given in table 2. The errors are difficult to estimate because of the large cross-correlations for this strongly coupled non-linear system [19]). They are obtained by requesting the total integrated probability within the error bounds to be equal to a confidence limit of 68.3%. Furthermore, there are sources of systematic error that must be considered. The uncertainty in the ^{208}Pb beam energy of 2% will have its largest effect on the high-spin states. For example, changing the beam energy from 916 MeV to 900 MeV will reduce the calculated $6_1^+ \rightarrow 4_1^+$ yield at the higher scattering angles by as much as 15%. To compensate for this, both the transitional and diagonal matrix elements

TABLE 1

Branching and mixing ratios in ^{114}Cd previously known from other experiments and used in the present analysis

$I_i \to I_1 / I_i \to I_2$	Branching ratio ref. [18])	Branching ratio present exp. [a])	Mixing ratio (δ) ref. [21])
$0_3^+ \to 2_2^+ / 0_3^+ \to 2_1^+$	1.76 ± 0.50	1.42 ± 0.48	
$0_4^+ \to 2_3^+ / 0_4^+ \to 2_1^+$	0.062 ± 0.010	0.064 ± 0.031	
$2_2^+ \to 2_1^+ / 2_2^+ \to 0_1^+$	3.03 ± 0.60	3.37 ± 0.31	−1.63 ± 0.20
$2_3^+ \to 2_1^+ / 2_3^+ \to 0_1^+$	1.14 ± 0.20	1.15 ± 0.58	0.05 ± 0.05
$2_3^+ \to 2_2^+ / 2_3^+ \to 0_1^+$	0.0019 ± 0.0004	0.0021 ± 0.0005	±1.95 ± 0.70
$2_3^+ \to 4_1^+ / 2_3^+ \to 0_1^+$	0.00010 ± 0.00005	0.00003 ± 0.00001 [b])	
$2_3^+ \to 0_2^+ / 2_3^+ \to 0_1^+$	0.027 ± 0.007	0.007 ± 0.001 [b])	
$2_4^+ \to 2_1^+ / 2_4^+ \to 0_1^+$	2.89 ± 0.50	2.4 ± 1.5	0.61 ± 0.30
$2_4^+ \to 2_2^+ / 2_4^+ \to 0_1^+$	0.14 ± 0.04	0.12 ± 0.08	
$2_4^+ \to 2_3^+ / 2_4^+ \to 0_1^+$	0.54 ± 0.10	0.67 ± 0.19	
$2_4^+ \to 0_2^+ / 2_4^+ \to 0_1^+$	1.88 ± 0.40	1.98 ± 0.47	
$2_4^+ \to 0_3^+ / 2_4^+ \to 0_1^+$	0.39 ± 0.10	0.51 ± 0.16	
$2_5^+ \to 2_1^+ / 2_5^+ \to 0_1^+$	13.3 ± 1.8	12.8 ± 4.9	
$2_5^+ \to 2_2^+ / 2_5^+ \to 0_1^+$	0.60 ± 0.13	0.58 ± 0.28	
$2_5^+ \to 0_3^+ / 2_5^+ \to 0_1^+$	1.33 ± 0.13	1.28 ± 0.48	
$4_2^+ \to 2_2^+ / 4_2^+ \to 2_1^+$	1.04 ± 0.30	1.33 ± 0.55	
$4_2^+ \to 2_3^+ / 4_2^+ \to 2_1^+$	0.71 ± 0.10	0.83 ± 0.17	
$4_2^+ \to 4_1^+ / 4_2^+ \to 2_1^+$	0.38 ± 0.10	0.25 ± 0.08	
$4_3^+ \to 2_3^+ / 4_3^+ \to 2_2^+$	0.35 ± 0.10	0.37	
$4_3^+ \to 4_1^+ / 4_3^+ \to 2_2^+$	0.66 ± 0.10	0.65	
$4_3^+ \to 4_2^+ / 4_3^+ \to 2_2^+$	0.026 ± 0.006	0.026	
$4_4^+ \to 4_1^+ / 4_4^+ \to 2_2^+$	0.63 ± 0.10	0.61	
$4_4^+ \to 4_2^+ / 4_4^+ \to 2_2^+$	0.37 ± 0.10	0.39	
$4_5^+ \to 4_2^+ / 4_5^+ \to 4_1^+$	0.045 ± 0.010	0.047	
$4_5^+ \to 4_3^+ / 4_5^+ \to 4_1^+$	0.025 ± 0.004	0.026	

The branching ratios, calculated from the measured matrix elements of the present experiment, also are given. The present data were insensitive to the matrix elements coupling to the 4_3^+, 4_4^+ and 4_5^+ states. Their absolute values therefore could not be measured, and the respective branching ratios were thus only adjusted by the code to fit the previous known branching ratios. Therefore, no errors are given for the branching ratios involving these states.

[a]) The present branching ratios are obtained from the fitted matrix elements. The fit partly makes use of the branching ratios of ref. [18]).

[b]) See footnote [g]) of table 2.

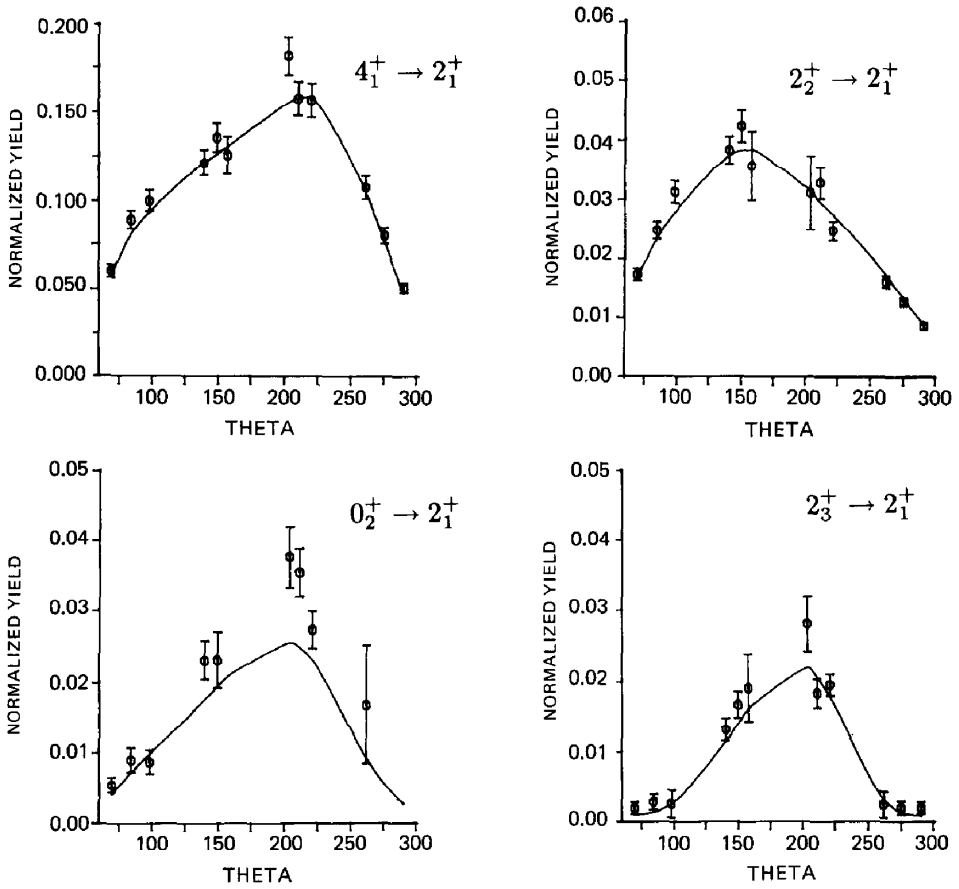

Fig. 7. A sample of the γ-ray yields for the left 155° Ge(Li) detector, in the Ni experiment, normalised to the $2_1^+ \rightarrow 0_1^+$ yield as a function of the centre-of-mass scattering angle. The scattering angles between 0° and 180° represent the two particle detectors to the left in fig. 2. Particles scattered to the right are represented by 180° to 360°. If the Ge detector would have been placed in 0° the curve would have been symmetric around 180° scattering. The solid curve is the corresponding calculated yield obtained with the best fit matrix elements.

must change about 8%. The same calculation for the 4^+ and the 2^+ states will only reduce their respective yields by about 5%, requiring at the most 2% change in their respective matrix elements. Also some higher order effects, discussed in sect. 4.10, may influence the result. The errors quoted in table 2, therefore, include an estimated uncertainty from systematic errors of 3% for the lower spin states. For the higher spin states, there are some additional sources of error as discussed in sect. 4.6. The 40 matrix elements determined in the present study have relative accuracies between 3% and 90%.

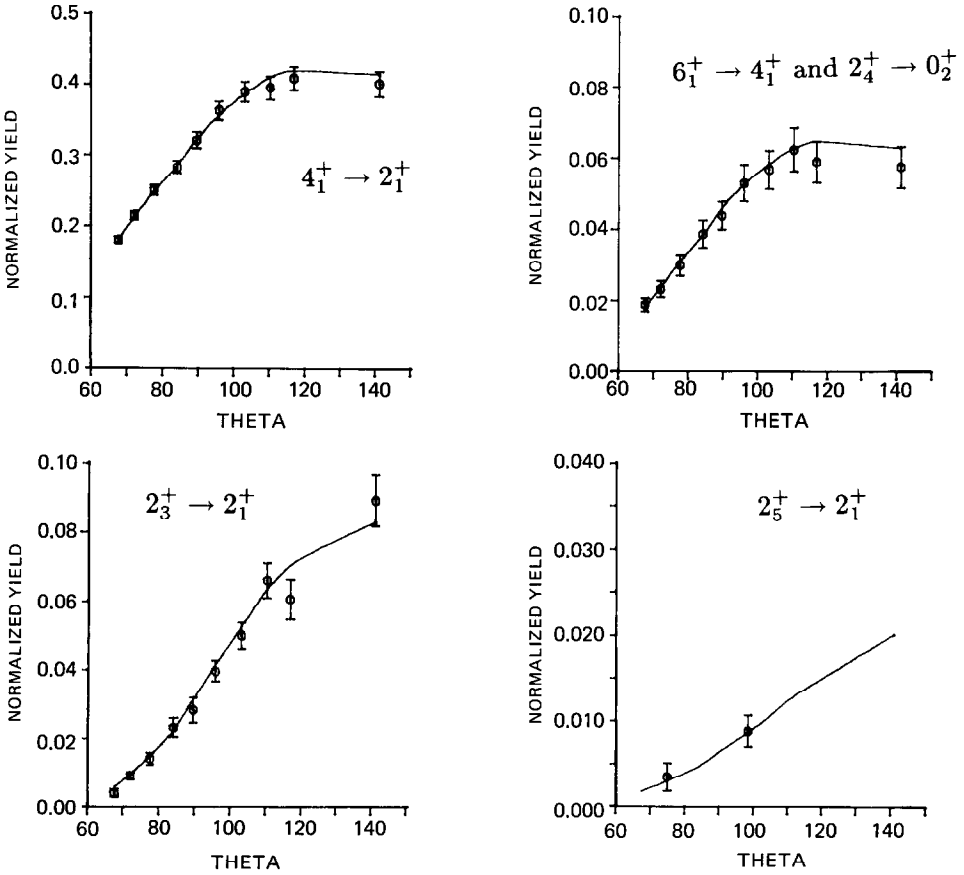

Fig. 8. A sample of the γ-ray yields for the 150° Ge(Li) detector, normalised to the $2_1^+ \rightarrow 0_1^+$ yield, in the Pb experiment, as a function of the centre-of-mass scattering angle. The solid curve is the corresponding calculated yield obtained with the best fit.

4.3. SENSITIVITY

The sensitivity of the excitation probability, P, to some of the matrix elements is illustrated with an example in fig. 9 for the 2_2^+ state. The sensitivity is defined as the relative change of P per relative change in matrix elements, i.e. $(\Delta P/P)/(\Delta M/M)$, and it is plotted as a function of the centre-of-mass scattering angle for the O, Ni and Pb bombardment. In the forward scattering direction of the O bombardment the excitation is taking place almost exclusively by the direct excitation to the 2_2^+ state. At more backward scattering angles the double excitation increases in importance. The rest of the matrix elements have negligible influence on $P(2_2^+)$. For the heavier projectiles it can be seen how higher-order excitation processes become more important. E.g. $\langle 2_2 \| M(\mathrm{E2}) \| 4_1 \rangle$ and $\langle 2_2 \| M(\mathrm{E2}) \| 2_2 \rangle$ start to

TABLE 2

Diagonal and transitional reduced E2 matrix elements in ^{114}Cd determined in the present experiment. Also listed are values of $B(E2)\downarrow$ from the present experiment and from previously known experiments.

Transition	Transition energy (MeV)	E2 matrix element ($e\cdot$b)	$B(E2)\downarrow$ (W.u.) [a]	$B(E2)\downarrow$ (W.u.) previous
$0_1^+ \rightarrow 2_1^+$	0.559	$0.714^{+0.021}_{-0.021}$	$31.0^{+1.9}_{-1.9}$	34.7 ± 4.1 [b])
				35.0 ± 1.4 [c])
				33.5 ± 1.2 [d])
$0_1^+ \rightarrow 2_2^+$	1.210	$0.091^{+0.003}_{-0.003}$	$0.50^{+0.04}_{-0.03}$	0.58 ± 0.09 [c])
$0_1^+ \rightarrow 2_3^+$	1.364	$0.073^{+0.003}_{-0.002}$	$0.33^{+0.02}_{-0.02}$	0.42 ± 0.08 [c])
$0_1^+ \rightarrow 2_4^+$	1.841	$0.056^{+0.005}_{-0.003}$	$0.19^{+0.04}_{-0.02}$	
$0_1^+ \rightarrow 2_5^+$	2.048	$0.042^{+0.003}_{-0.009}$	$0.11^{+0.01}_{-0.04}$	
$0_2^+ \rightarrow 2_1^+$	0.576	$0.300^{+0.007}_{-0.009}$	$27.3^{+1.3}_{-1.6}$	29.9 ± 5.6 [b])
				41 ± 8 [e])
$0_2^+ \rightarrow 2_2^+$	0.075	$-0.17^{+0.04}_{-0.02}$	$1.8^{+0.9}_{-0.4}$	
$0_2^+ \rightarrow 2_3^+$	0.229	$0.51^{+0.03}_{-0.03}$	16^{+2}_{-2} [g])	
$0_2^+ \rightarrow 2_4^+$	0.706	$0.86^{+0.05}_{-0.05}$	45^{+5}_{-5}	
$0_3^+ \rightarrow 2_1^+$	0.747	$0.00300^{+0.00045}_{-0.00014}$	$0.0027^{+0.0009}_{-0.0003}$	0.0038 ± 0.0005 [e])
$0_3^+ \rightarrow 2_2^+$	0.096	$0.60^{+0.02}_{-0.02}$	109^{+8}_{-8}	101 ± 7 [e])
$0_3^+ \rightarrow 2_3^+$	0.058	$0.33^{+0.06}_{-0.08}$	$6.6^{+2.6}_{-2.8}$	
$0_3^+ \rightarrow 2_4^+$	0.535	$0.87^{+0.10}_{-0.03}$	46^{+11}_{-3}	
$0_3^+ \rightarrow 2_5^+$	0.742	$0.61^{+0.03}_{-0.03}$	$22.6^{+2.3}_{-2.2}$	
$0_4^+ \rightarrow 2_1^+$ [k])	1.301	$0.09^{+0.01}_{-0.01}$	$2.5^{+0.5}_{-0.6}$	
$0_4^+ \rightarrow 2_3^+$ [k])	0.496	$-0.26^{+0.05}_{-0.02}$	21^{+9}_{-3}	
$0_4^+ \rightarrow 2_5^+$ [k])	0.188	$1.45^{+0.06}_{-0.36}$	128^{+10}_{-56}	
$2_1^+ \rightarrow 2_1^+$		$-0.36^{+0.01}_{-0.03}$		
$2_1^+ \rightarrow 2_2^+$	0.651	$0.684^{+0.021}_{-0.021}$	$28.4^{+1.8}_{-1.7}$	24.6 ± 7.0 [c])
				24 ± 7 [f])
$2_1^+ \rightarrow 2_3^+$	0.805	$0.025^{+0.011}_{-0.005}$	$0.04^{+0.01}_{-0.02}$	$0.02^{+0.13}_{-0.02}$ [f])
$2_1^+ \rightarrow 2_4^+$	1.282	$-0.08^{+0.02}_{-0.01}$	$0.38^{+0.23}_{-0.08}$	
$2_1^+ \rightarrow 2_5^+$ [h])	1.489	$0.33^{+0.02}_{-0.01}$	$6.6^{+0.8}_{-0.4}$	
$2_1^+ \rightarrow 4_1^+$	0.725	$1.35^{+0.04}_{-0.04}$	$61.5^{+3.8}_{-3.5}$	64.1 ± 7.4 [b])
$2_1^+ \rightarrow 4_2^+$	1.173	$0.11^{+0.01}_{-0.01}$	$0.41^{+0.07}_{-0.07}$	
$2_2^+ \rightarrow 2_2^+$		$0.92^{+0.04}_{-0.05}$		
$2_2^+ \rightarrow 2_3^+$ [i])	0.154	$0.71^{+0.02}_{-0.09}$	31^{+2}_{-7}	
$2_2^+ \rightarrow 2_4^+$ [h])	0.631	$0.28^{+0.04}_{-0.06}$	$4.8^{+1.4}_{-2.9}$	
$2_2^+ \rightarrow 2_5^+$ [h])	0.838	$-0.28^{+0.04}_{-0.05}$	$4.8^{+1.4}_{-1.6}$	
$2_2^+ \rightarrow 4_1^+$	0.074	$-0.35^{+0.07}_{-0.02}$	$4.1^{+1.8}_{-0.4}$	
$2_2^+ \rightarrow 4_2^+$	0.522	$0.97^{+0.17}_{-0.03}$	32^{+12}_{-2}	
$2_3^+ \rightarrow 2_3^+$		$0.29^{+0.10}_{-0.27}$		
$2_3^+ \rightarrow 2_4^+$ [h])	0.477	$-1.33^{+0.10}_{-0.14}$	107^{+17}_{-21}	
$2_3^+ \rightarrow 4_1^+$	0.080	$0.46^{+0.06}_{-0.02}$	$12.9^{+3.5}_{-1.2}$ [g])	
$2_3^+ \rightarrow 4_2^+$	0.368	$1.85^{+0.10}_{-0.06}$	115^{+13}_{-8}	
$4_1^+ \rightarrow 4_1^+$		$-0.95^{+0.04}_{-0.11}$		
$4_1^+ \rightarrow 4_2^+$	0.448	$0.61^{+0.08}_{-0.04}$	$12.6^{+3.4}_{-1.7}$	
$4_1^+ \rightarrow 6_1^+$	0.707	$2.26^{+0.34}_{-0.34}$	119^{+39}_{-33}	
$4_2^+ \rightarrow 6_2^+$	0.668	$2.35^{+0.35}_{-0.35}$ [j])	129^{+42}_{-35}	
$6_1^+ \rightarrow 6_1^+$		$-3.49^{+0.87}_{-0.87}$		
$6_1^+ \rightarrow 8_1^+$	0.679	$2.19^{+0.33}_{-0.33}$ [j])	86^{+28}_{-24}	

have an influence already with the Ni beam and with back-scattered Pb ions about 10 matrix elements are of importance for the excitation of the 2_2^+ state, not all of them shown in fig. 9. The necessity to measure the Coulomb excitation yields over a wide range of interaction strength is obvious.

It is very interesting to note, that the above matrix elements, coupled to the 2_2^+ state, also have an influence on the excitation probability of other states. This is illustrated in fig. 10, where the sensitivity of the 2_3^+ state is plotted for the same matrix elements as in fig. 9. A very dramatic dependence is observed for $\langle 0_1 \| M(\mathrm{E2}) \| 2_2 \rangle$ and $\langle 2_1 \| M(\mathrm{E2}) \| 2_2 \rangle$.

Fig. 11 shows the sensitivity of some of the matrix elements to the 2_2^+ state in a somewhat different way. In this figure the γ-ray yield of the $2_2^+ \rightarrow 2_1^+$ transition, normalized to the $2_1^+ \rightarrow 0_1^+$ transition, is plotted as a function of the centre-of-mass scattering angle for the Ca and Pb experiments. The curve called 'best fit' is the calculated yield obtained with the matrix elements given in table 2. The other curves are obtained by simply changing the sign of the matrix elements indicated to the right of the curves. In the Ca experiment the yield is rather insensitive to most of the signs of the matrix elements, as well as to their magnitudes which were tested similarly, except to that of the quadrupole moment of the state itself. The Pb experiment is sensitive to the static quadrupole moment as well as to $\langle 2_2 \| M(\mathrm{E2}) \| 4_1 \rangle$ and $\langle 0_3 \| M(\mathrm{E2}) \| 2_2 \rangle$, which are the E2 couplings between some close-lying levels within the quintuplet. Thus they can be determined without actually observing the respective γ-transitions. Combining all the yields and their different sensitivities as a function of the interaction strength makes it possible to determine the E2 matrix elements involved. Short comments on individual results are described below.

4.4. THE 2_1^+ STATE

The first excited 2^+ state has been subject to many studies. Its $B(\mathrm{E2})$ value to the ground state is well known [25]), and its quadrupole moment has been determined in

---

[a]) 1 W.u. $= 5.94 \times 10^{-6} A^{4/3} e^2 b^2$

[b]) Ref. [22]).

[c]) Ref. [23]).

[d]) Ref. [25]).

[e]) Ref. [10]).

[f]) Ref. [24]).

[g]) The previously known branching ratios (see table 1), suggest the $B(\mathrm{E2})\downarrow$ of the $0_2^+ \rightarrow 2_3^+$ transition to be 67 W.u. and that of the $2_3^+ \rightarrow 4_1^+$ transition to be 48 W.u. However, it is not possible to fit the present Coulomb excitation data, with such large values of these two transitions.

[h]) The E2 matrix element is obtained assuming no M1 admixture.

[i]) The E2 matrix element is obtained assuming $\delta = -1.95$ (see table 1). The same χ^2 is obtained with $\delta = +1.95$.

[j]) Obtained assuming the 668 keV γ-ray to be the $8_1^+ \rightarrow 6_1^+$ transition and the 679 keV γ-ray to be the $6_2^+ \rightarrow 4_2^+$ transition.

[k]) The matrix element is uncertain because of the influence from uncertain signs of interference terms.

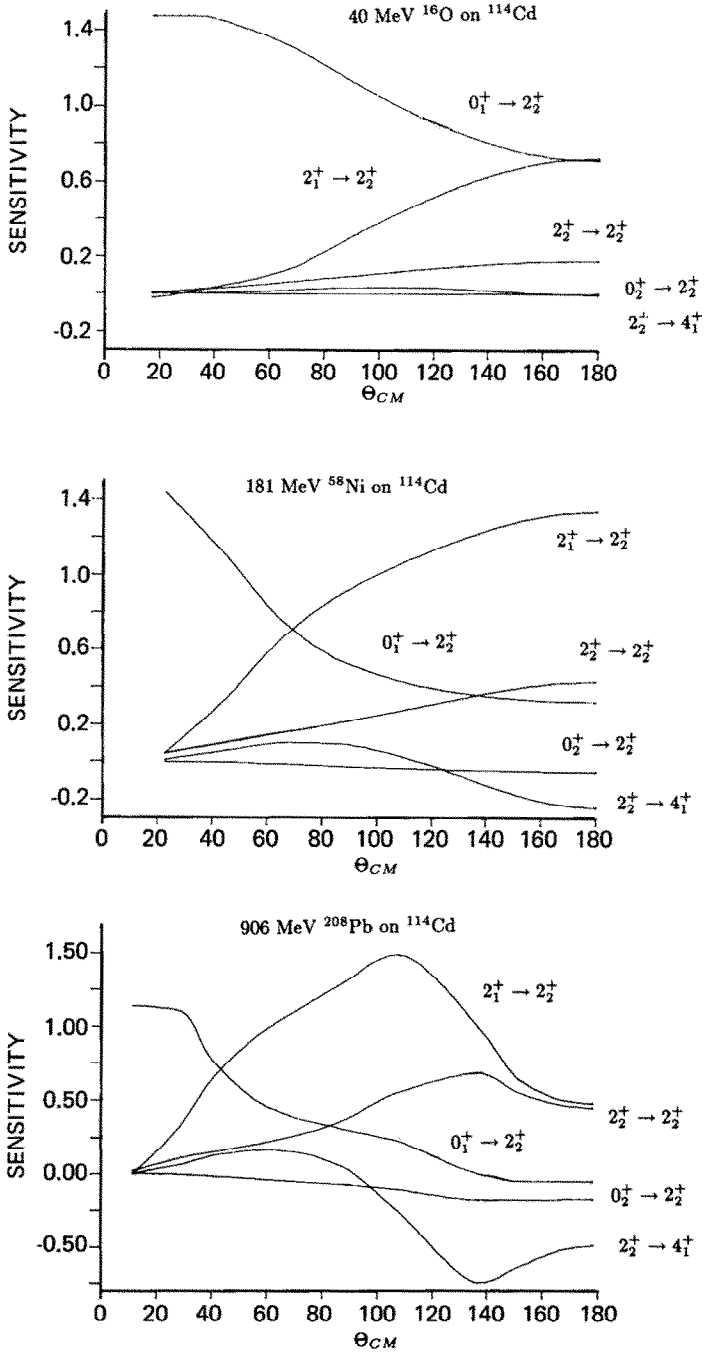

Fig. 9. The sensitivity of the excitation probability $((\Delta P/P)/(\Delta M/M))$ of the 2_2^+ state for the O, Ni and Pb experiments, for some selected matrix elements.

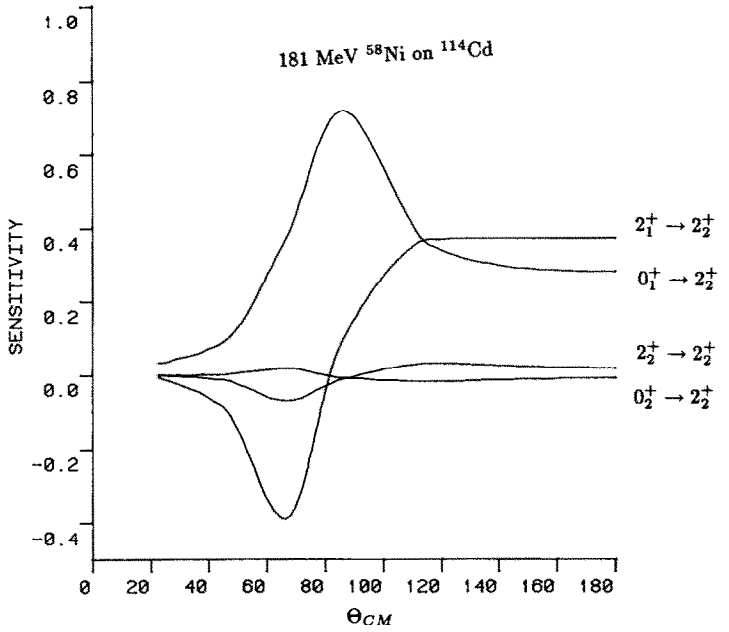

Fig. 10. The sensitivity of the excitation probability $((\Delta P/P)/(\Delta M/M))$ of the 2_3^+ state for the Ni experiment, for the same matrix elements as in fig. 9.

reorientation measurements. A weighted mean of the recent reorientation measurements [26-30]) gives a value of the quadrupole moment of $Q(2_1^+) = -0.36 \pm 0.03\ e \cdot \text{b}$. Note that the static moment $Q(2_1^+) = 0.758\langle 2_1 \| M(\text{E2}) \| 2_1 \rangle$. The quadrupole moment obtained in the present experiment is somewhat smaller, $Q(2_1^+) = -0.27^{+0.01}_{-0.02}\ e \cdot \text{b}$.

4.4. THE 2_1^+ STATE

The first excited 2^+ state has been subject to many studies. Its $B(\text{E2})$ value to the ground state is well known [25]), and its quadrupole moment has been determined in several reorientation measurements [26-30]). A weighted mean of these experiments gives a value of $Q(2_1^+) = -0.36 \pm 0.03$ eb. Note that the static moment $Q(2_1^+) = 0.758\langle 2_1 \| M(\text{E2}) \| 2_1 \rangle$. The quadrupole moment obtained in the present experiment is somewhat smaller, $Q(2_1^+) = -0.27^{+0.01}_{-0.02}\ e \cdot \text{b}$.

4.5. THE QUINTUPLET OF STATES AT ABOUT 1.2 MeV

There are 19 E2 matrix elements and 3 M1 matrix elements involved in the deexcitation of the quintuplet of states. The δ-values for the mixed E2/M1 transitions are known (table 1) and included in the analysis. The magnitudes of all 19 E2 matrix elements are determined unambiguously and are given in table 2. This includes the E2 matrix elements between states within the quintuplet and the quadrupole moments

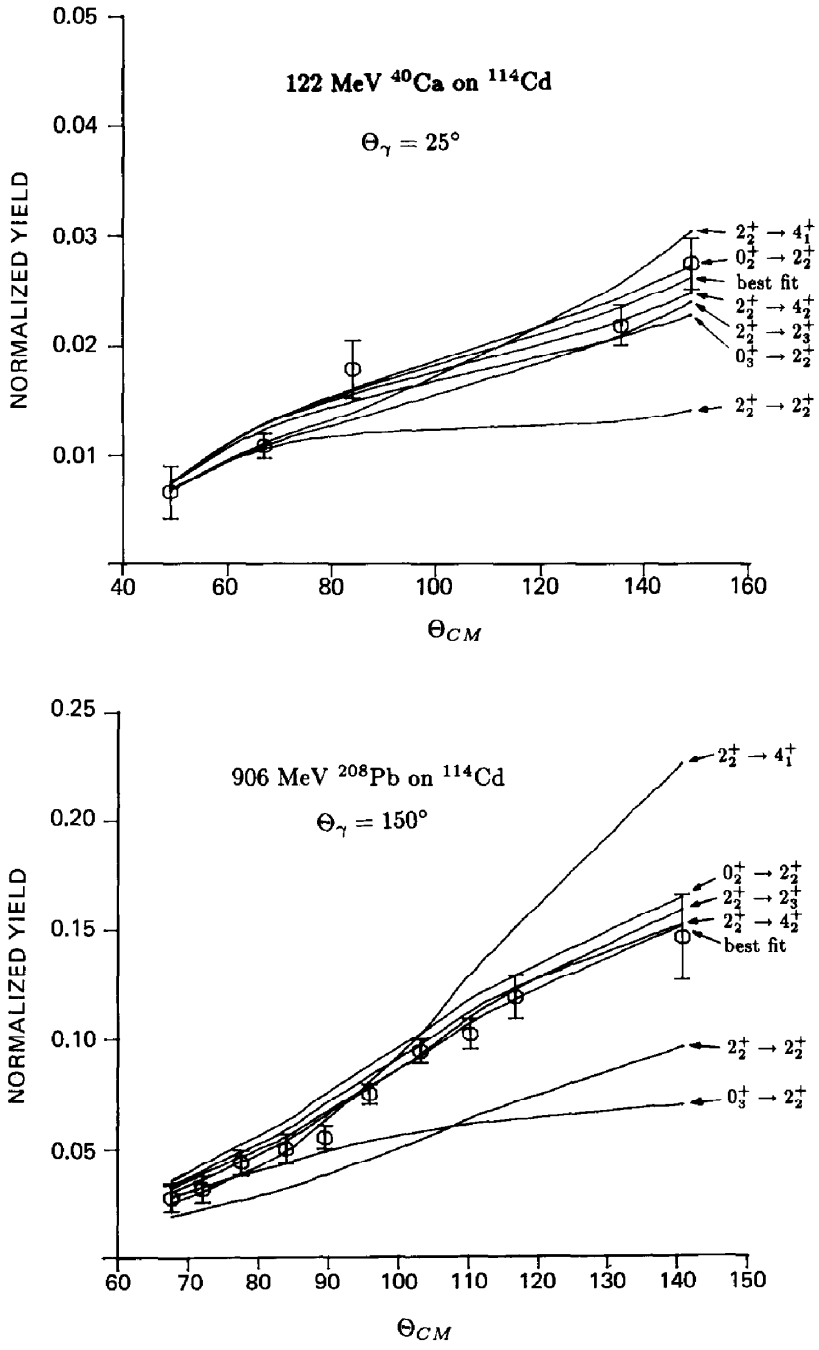

Fig. 11. The influence of the γ-ray yield of the $2_2^+ \rightarrow 2_1^+$ transition (normalised to the $2_1^+ \rightarrow 0_1^+$ transition) for the Ca and Pb experiments, to a change of sign of the matrix elements indicated.

of the 4_1^+, 2_2^+ and 2_3^+ states. The signs of 5 of the E2 matrix elements can be chosen arbitrarily (fig. 6). Two of the signs are insensitive to the data and the remaining 12 are determined relative to the first 5. It is possible that a different sign combination together with a set of different magnitudes of the matrix elements also may give rise to a good fit. Therefore several different sign combinations were tried by simply changing them one by one by hand. In all cases this increased the χ^2 value drastically and in the further minimization it was not possible to reach as good a minimum as obtained originally with the matrix elements of table 2. Of course there are restrictions with respect to the magnitudes of the matrix elements, because of the conditions posed by the known branching ratios included in the analysis. It is concluded that the combination of the present data with the previously known branching ratios is sufficient to uniquely determine all E2 matrix elements with relative signs for the quintuplet.

The sign of the quadrupole moment of the 2_2^+ state is positive. This can be seen in the Ca experiment in fig. 11, where a negative sign of $\langle 2_2 \| M(\mathrm{E2}) \| 2_2 \rangle$ significantly distorts the fit. It was not possible to reproduce the fit with any of the other matrix elements involved. The magnitude is determined to be 0.92 $e \cdot$ b with an uncertainty of only 5%. Such a good accuracy is obtained because there are many data points with accuracies between 5 and 10% that are sensitive to $\langle 2_2 \| M(\mathrm{E2}) \| 2_2 \rangle$, and because the number of cross-correlations is relatively small, making the system very much overdetermined. The same is true for the quadrupole moment of the 4_1^+ state. The quadrupole moment of the 2_3^+ state on the other hand could not be determined to better than about 90%. This is due to the fact that the statistics is poorer, it is less sensitive to the data, the number of cross-correlations is larger and there are fewer data points which involve the excitation of the 2_3^+ state.

4.6. THE 6_1^+ STATE

The first 6^+ state has not been observed previously. In the present experiment it has tentatively been assigned to an energy of 1.991 MeV. The evidence for this assignment is rather strong as discussed in sect. 3. However, the corresponding 707 keV γ-ray transition to the 4_1^+ state contains a component from the $2_4^+ \rightarrow 0_2^+$ transition and therefore it is treated as a doublet in the analysis. The fit to the doublet is shown in fig. 8 for the 150° Ge(Li) detector in the Pb experiment. The γ-ray yield increases with scattering angle up to about 110°, where it levels off and then decreases slightly at larger scattering angles. This drop in yield is reproduced by a large negative value of the quadrupole moment of the 6_1^+ state.

The $\langle 6_1 \| M(\mathrm{E2}) \| 4_1 \rangle$ and $\langle 6_1 \| M(\mathrm{E2}) \| 6_1 \rangle$ matrix elements dominate the excitation of the 6_1^+ state. The interference terms $\langle 4_1 \| M(\mathrm{E2}) \| I_r \rangle \langle I_r \| M(\mathrm{E2}) \| 6_1 \rangle \langle 6_1 \| M(\mathrm{E2}) \| 4_1 \rangle$ coupling to the 6_1^+ state are not known and cannot be determined with the present data. A destructive interference, i.e. a negative sign of the product, will have the same effect on the γ-yield as a negative quadrupole moment. Thus an increase of

the magnitude of a destructive interference term will cause a drop in the yield thus requiring a corresponding reduction of $\langle 6_1 \| M(E2) \| 6_1 \rangle$. All possible such couplings have been checked and it is found that only the products with $I_r = 4_2$ and $I_r = 6_2$ are important, although their sensitivity to the data still is much smaller than that of the quadrupole moment. However, the uncertainty of the interference terms adds to the uncertainty of the quadrupole moment.

The small component of the $2_4^+ \rightarrow 0_2^+$ transition in the 707 keV γ-ray, although it is partly taken care of by the code, may also add to the uncertainty of $\langle 4_1 \| M(E2) \| 6_1 \rangle$ and $\langle 6_1 \| M(E2) \| 6_1 \rangle$, as well as the error from the beam energy as discussed in sect. 4.2. The total errors are estimated to be 15% and 25%, respectively.

4.7. THE 0_4^+, 2_4^+ AND 2_5^+ STATES

The transitions $2_4^+ \rightarrow 2_1^+$ of 1282 keV and $2_5^+ \rightarrow 2_1^+$ of 1489 keV are observed in the summed windows of the Pb experiment. The branching ratios from these states are well known, but the mixing ratio is known only for the $2_4^+ \rightarrow 2_1^+$ transition. The rest of the E2 matrix elements from the decay of the 2_4^+ and 2_5^+ states are determined assuming the transitions to be pure E2. However, including for these transitions an M1 admixture of the same magnitude as for the $2_2^+ \rightarrow 2_1^+$ transition, has negligible influence on the extraction of the corresponding E2 matrix elements.

The 2_5^+ state is more strongly populated than the 2_4^+ state (see fig. 4). It is found that the unobserved 0_4^+ state is very important for the excitation of the 2_5^+ state, through the $0_1^+ \rightarrow 2_1^+ \rightarrow 0_4^+ \rightarrow 2_5^+$ excitation path. A large matrix element is necessary between the 0_4^+ and 2_5^+ states to account for the 2_5^+ population. The sensitivity of the E2 couplings to the 0_4^+ state was tested by setting the respective E2 matrix elements equal to zero. This reduced the intensity of the $2_5^+ \rightarrow 2_1^+$ transition by one order of magnitude. In order to reproduce this intensity without the 0_4^+ state involved, the other E2 matrix elements coupled to the 2_5^+ state had to be increased by a factor of 3, or a factor of 9 in the $B(E2)$ values, which is unrealistically large. Furthermore, such a big change of the E2 matrix elements to the 2_5^+ state, has an effect on the population of other states coupled to the 2_5^+ state, and the overall fit is not as good any longer. Thus it is concluded that the 0_4^+ state must be involved and 3 matrix elements coupled to this state were determined. However, one must be somewhat cautious since the excitation to these states involve about 15 matrix elements and the number of experimental data points is relatively small. Although the relative magnitudes between 12 of these matrix elements are known by their corresponding branching ratios, it cannot be disregarded that a different sign combination may alter the magnitudes, particularly of the matrix elements coupled to the 0_4^+ state.

4.8. THE 4_2^+ AND 4_5^+ STATES

The 4_2^+ and the 4_5^+ states were observed in the Pb experiment, whereas the 4_3^+ and 4_4^+ were not. The 4_2^+ state decays mainly to the three lower 2^+ states, but its branching ratio to the 4_1^+ state is also known. The matrix elements involved in the

deexcitation of the 4_2^+ state have an influence on the excitation of other close-lying states, e.g. the 2_2^+ and 2_3^+ states, and they are well determined in the present experiment.

The 4_5^+ state is populated almost as strong as the 4_2^+ state (fig. 4). However, the situation for the 4_5^+ state is different. It is excited through as many different paths as to the 4_2^+ state, but to the latter state there is only a few dominating matrix elements involved, and to the 4_5^+ state there are several paths with similar importance, involving many unknown matrix elements. Further, there are many possibilities for decay, the branching is only partly known, and only in two of the 30 experimental sets of yields, are the yields measured for the $4_5^+ \rightarrow 4_1^+$ transition, which furthermore appears to be a doublet (fig. 4). The second γ-ray line may be the $6_2^+ \rightarrow 4_1^+$ transition, which only differs by 8 keV, assuming that the 668 keV transition is the $6_2^+ \rightarrow 4_2^+$ transition (see sect. 4.9). Therefore, it is not possible to determine unambiguously the E2 matrix elements involved in the decay of the 4_5^+ state.

The unobserved lower-lying 4_3^+ and 4_4^+ states were included in the analysis. The reason why the 4_3^+ state is not observed may be found in the fact that its strongest transitions, the $4_3^+ \rightarrow 2_2^+$ with an energy of 722 keV, the $4_3^+ \rightarrow 4_1^+$ with energy 648 keV and the $4_3^+ \rightarrow 2_3^+$ with energy 568 keV, are hidden by the much stronger 725, 651 and 559 keV lines, respectively (see table 2). The matrix elements coupled to these two states were allowed to vary during the final minimisation, but their sensitivity to the data was very weak and it was not possible to determine them.

4.9. THE TENTATIVE 8_1^+ AND 6_2^+ STATES

Two γ-rays with energies of 668 and 679 keV were observed with an intensity of the first γ-ray line about 40% stronger than the latter. They have tentatively been assigned as the $6_2^+ \rightarrow 4_2^+$ and $8_1^+ \rightarrow 6_1^+$ transitions. The excitation probabilities of these states are mainly determined by their respective "in-band" matrix elements and the correlations are relatively weak. The errors for the $\langle 6_1 \| M(\mathrm{E2}) \| 8_1 \rangle$ and $\langle 4_2 \| M(\mathrm{E2}) \| 6_2 \rangle$ matrix elements are estimated to be 15% for the same reasons as discussed in sect. 4.6, and, with the above assumption, values of 2.35(40) and 2.19(33) $e \cdot \mathrm{b}$ were obtained, respectively. With the opposite assumption, the $\langle 6_1 \| M(\mathrm{E2}) \| 8_1 \rangle$ matrix element is increased by about 20% and the $\langle 4_2 \| M(\mathrm{E2}) \| 6_2 \rangle$ matrix element reduced by about the same amount.

4.10. CORRECTIONS

There are several higher order effects that may have an influence on the extracted E2 matrix elements. The virtual excitation of the giant dipole resonance is taken into account in the code according to the prescription of Alder and Winther [31]). It has the largest effect on the higher lying states, and switching it off entirely changes e.g. the $6_1^+ \rightarrow 4_1^+$ yield by as much as 6%.

The de-orientation effect is also taken into account using the two-state model of Brenn *et al.* [32]). Its largest effect is on the long-lived states, in this case mainly the

first 2^+ state. A detailed study of the influence of the de-orientation effect on the extracted E2 matrix elements is given by Wu [33]). It is found there that an uncertainty as large as 20% in the parameters of the two-state model generally produces a less than 2% change in the extracted matrix elements.

To test the influence of a possible hexadecapole deformation the matrix element $\langle 0_1 \| M(\mathrm{E4}) \| 4_1 \rangle$ was introduced. Even with a relatively large value of 0.10 $e \cdot \mathrm{b}^2$ (about 6 W.u.), the influence on the $4_1^+ \rightarrow 2_1^+$ yield was only about 1% for the most sensitive experiment, producing an even smaller change in the corresponding E2 matrix elements. Similarly the influence of the 3^- state, which was excited in the ^{16}O experiment, was tested. The previously known value [22]) of $\langle 3_1^- \| M(\mathrm{E3}) \| 0_1^+ \rangle = 0.30\ e \cdot \mathrm{b}^{3/2}$ was included. The E1 branching to the 2_1^+ state has been measured in ^{116}Sn [ref. [5])] and the E1 strength was found to be hindered by a factor 10^3. Assuming the same hindrance in ^{114}Cd, the experimental yield of the $3_1^- \rightarrow 2_1^+$ transition was reproduced in the ^{16}O experiment, but there was no influence on any of the other yields.

Coulomb excitation of unnatural parity states, such as the 3_1^+ state, is negligible because destructive interference occurs between the major multiple-excitation pathways and also the normally low-order Coulomb excitation terms are forbidden by selection rules for such states. Population of such unnatural parity states occurs primarily due to γ-ray feeding following Coulomb excitation. In the present experiment the 3_1^+ state at 1864 keV was not observed, but its influence was tested by including it together with realistic values of the corresponding E2 matrix elements and it was found to have a negligible effect on the rest of the E2 matrix elements.

The quantum mechanical effects are difficult to deal with when heavy ions are used, and no such corrections have been applied to the present analysis. The quantal effects are expected to be largest for the bombardment with ^{16}O, since the correction varies as $1/\eta$, where η is the Sommerfeld parameter. In the ^{16}O experiment no γ-yields were measured to better than 15%, and the quantal corrections are expected to lie within the experimental yields.

5. Sum rule calculations

The large number of experimental E2 matrix elements can be summarised by means of a sum-rule method, first suggested by Kumar [34]). In the present paper the Cline-Flaum sum-rule method [35]) is applied. By this method it is possible to project directly the expectation values of the E2 properties in the intrinsic principal axis frame of reference for all states for which a complete set of E2 matrix elements has been measured. Cline and Flaum define the expectation values of the E2 operators in this frame of reference by specifying two parameters, Q and δ, which are analogous to Bohr's quadrupole shape parameters β and γ. The zero-coupled products of the spherical tensor E2 operators are rotationally invariant and their expectation values

for a state can be expressed in terms of the intrinsic frame E2 parameters Q and δ. Furthermore, the expectation values of these parameters can be evaluated as sums of products of E2 matrix elements in the laboratory frame by making intermediate-state expansions of the rotationally invariant products. For those states, for which all matrix elements that contribute to the sum rule are measured, it is thus possible to obtain the intrinsic parameters Q and δ. The calculation is completely independent of any nuclear model assumptions. For further details, see refs. [36,37]).

The method has been applied successfully to several nuclei in the rare-earth region [37]), and to ^{110}Pd [ref. [9])]. In the case of ^{114}Cd, the present data allow only the sum rule to be applied to lowest order, thus determining only the expectation values Q^2. The result of this calculation is shown in fig. 12. The straight lines in the figure are obtained by applying the sum rule to the matrix elements of a pure harmonic vibrator. The sum rule applied to a rigid rotor would give a horizontal line in this type of plot. The values of Q^2 obtained from the experimental matrix elements represent a lower limit, since the lowest-order expectation value is just the sum of all B(E2) values coupled to the state in question, and therefore any missing E2 coupling can only increase the values of Q^2. The expectation value of Q^2 for the ground state is calculated to 0.53 (1) e^2b^2 ($\beta = 0.17$), which increases for the 0_2^+ state to $Q^2 = 1.1$ (1) e^2b^2 ($\beta = 0.25$) and for the 0_3^+ state to $Q^2 = 1.5$ (2) e^2b^2 ($\beta = 0.30$). For the 0_4^+ state a value of $Q^2 = 2.1$ (7) ($\beta = 0.34$) is obtained. However, this value is somewhat uncertain, because of the uncertainty in the matrix elements involved in the coupling to the 0_4^+ state as discussed in sect. 4.7. For the higher spin states the values may be somewhat low, since not all E2 couplings may be known, but

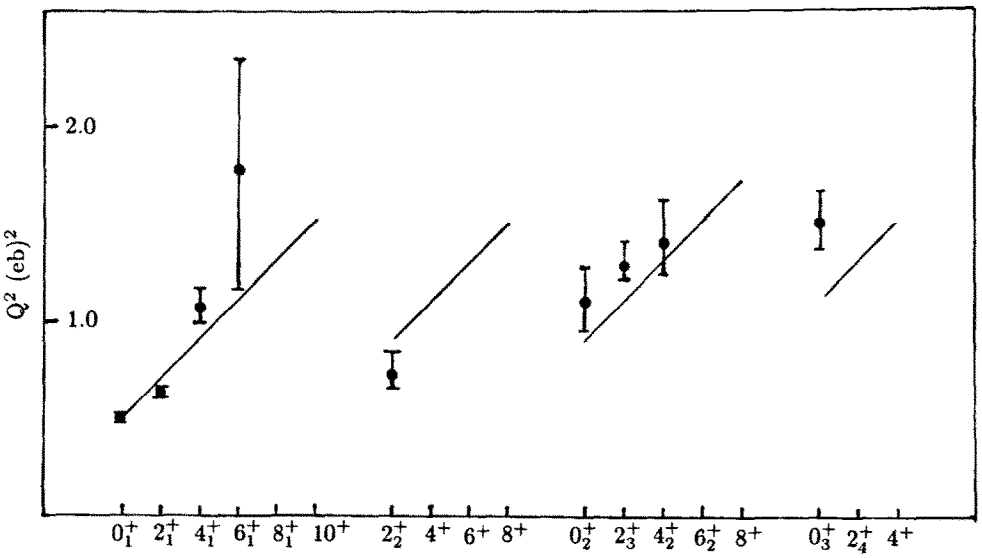

Fig. 12. The expectation value Q^2 of the sum-rule calculation as a function of spin in ^{114}Cd.

the missing couplings are very likely to be small. The results indicate that vibrational motion plays a significant rule in ^{114}Cd. This calculation will be commented on further in the following sections.

The sum rule expression for the expectation value of δ, and the higher order sum rules, which describe the distribution in the Q-δ plane, and which can be related to the softness in the β- and γ-directions if so desired, are much more complicated and therefore more sensitive to missing strength due to incomplete summation, as well as being sensitive to the signs of the matrix elements. These sum rule expressions are not well determined in the present case except for the 0_1^+ state where $\delta = 27\ (2)°$.

6. Discussion

6.1. ^{114}Cd AS A VIBRATIONAL NUCLEUS

The collective low-energy excitations of ^{114}Cd show several features typical of a spherical vibrator. Fig. 13 shows the level structure of a pure harmonic vibrator up to the 4-phonon state, which has 8 degenerate levels. When compared to the ^{114}Cd level structure it is interesting to note that these phonon states almost completely exhaust the experimentally known levels below an energy of about 2.6 MeV (see figs. 5 and 13). The splitting of the energies of the 2-phonon triplet may be explained by a small anharmonic term in the vibration. The 3-phonon state shows a much larger energy splitting of the levels, where the low-spin 0_3^+ and 2_3^+ states are lowered in energy and the 3^+, 4^+ and 6^+ states are increased in energy. A similar large splitting also occurs for the 4-phonon levels, with the 6^+ and 8^+ states higher in energies and the lower-spin states lowered in energies.

In principle it is possible to arrange the levels of the harmonic vibrator in bands, in which the levels are connected with large B(E2) values. The resulting band structure is shown in fig. 14 for some of the levels up to the 6-phonon state. The numbers in the figure are the relative B(E2) values of the harmonic vibrator, normalised to the experimental value of the $2_1^+ \rightarrow 0_1^+$ transition in ^{114}Cd, which is 31 Weisskopf units (W.u.). The experimental B(E2) values are given in table 2 and some of them are included within brackets in fig. 14. As seen in the figure, several of these values are in reasonable agreement with the harmonic vibrator picture. The B(E2) value of the $4_1^+ \rightarrow 2_1^+$ transition has a strength of 62 W.u., which is twice the strength of the $2_1^+ \rightarrow 0_1^+$ transition. The values of $B(\mathrm{E2}; 0_2^+ \rightarrow 2_1^+)$ and $B(\mathrm{E2}; 2_2^+ \rightarrow 2_1^+)$ are of the predicted order of magnitude for vibrator transitions, although somewhat too small. The interpretation of the 0_2^+ state as being vibrational is supported by its E0 decay [10,20]. The ratio, $X = B(\mathrm{E0}; 0_2^+ \rightarrow 0_1^+)/B(\mathrm{E2}; 0_2^+ \rightarrow 2_1^+)$, is 0.026, which is of similar magnitude as the spherical vibrator value of 0.036. Further, the value of $B(\mathrm{E2}; 6_1^+ \rightarrow 4_1^+)$ is about three times the 1-phonon strength, which supports the interpretation of the 6_1^+ state as a possible member of the 3-phonon multiplet. The E2 decay of the 0_3^+ and 2_3^+ states at 1.306 and 1.364 MeV respectively, to the 2_1^+

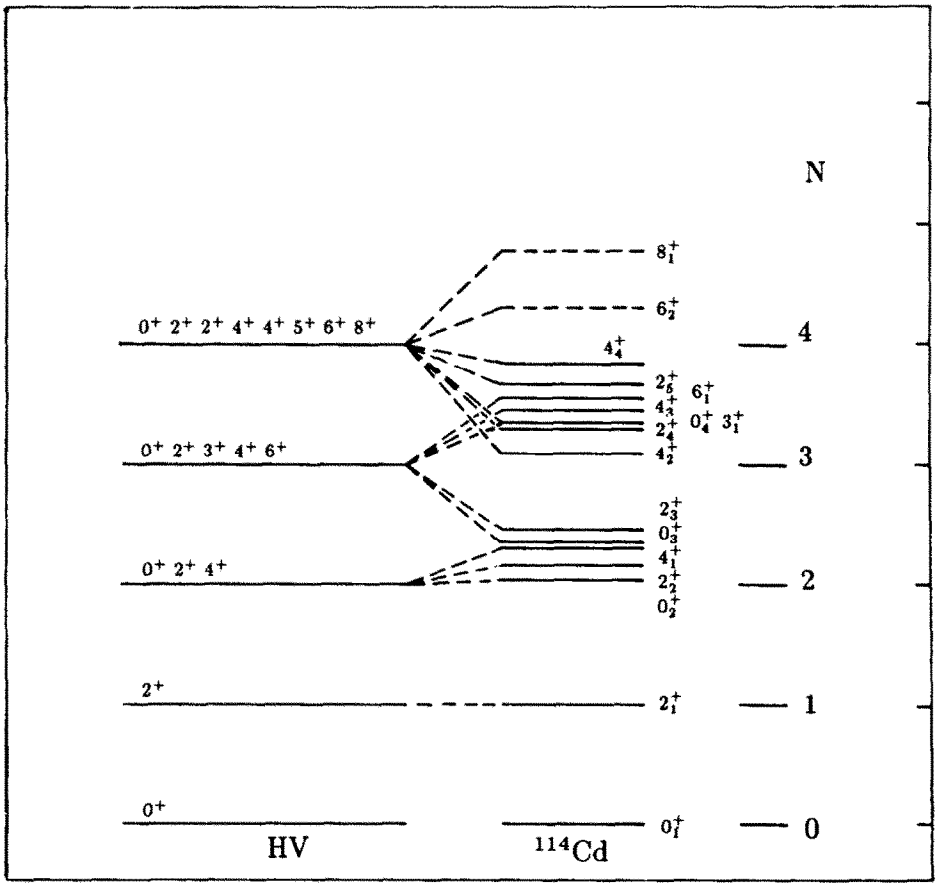

Fig. 13. The level structure of a harmonic vibrator up to phonon number $N = 4$ compared with the levels of ^{114}Cd.

state are both hindered as compared to the single-particle strength, the 0_3^+ state by more than a factor of 300. This is in accordance with an interpretation in terms of 3-phonon states, since in the harmonic vibrator picture $\Delta N = 2$ transitions are forbidden. It also explains the strongly enhanced $0_3^+ \to 2_2^+$ and $2_4^+ \to 0_3^+$ transitions. The other $B(E2)$ values indicated in the figure are also in fair agreement with the harmonic vibrator values. Thus there is a considerable amount of experimental data supporting the idea of a vibrational structure, including the sum-rule calculation as shown in the previous section.

The surprisingly large quadrupole moment of the first excited 2^+ state, measured first in 1965 [38]) could be explained by a small anharmonic term in the vibrational potential. The $B(E2)$ values calculated for a potential with an anharmonicity of about 2% are discussed in sect. 6.3, and the result is shown in table 3 of that section. The $B(E2)$ values of the $2_2^+ \to 0_2^+$ and $4_1^+ \to 2_2^+$ transitions, within the 2-phonon triplet,

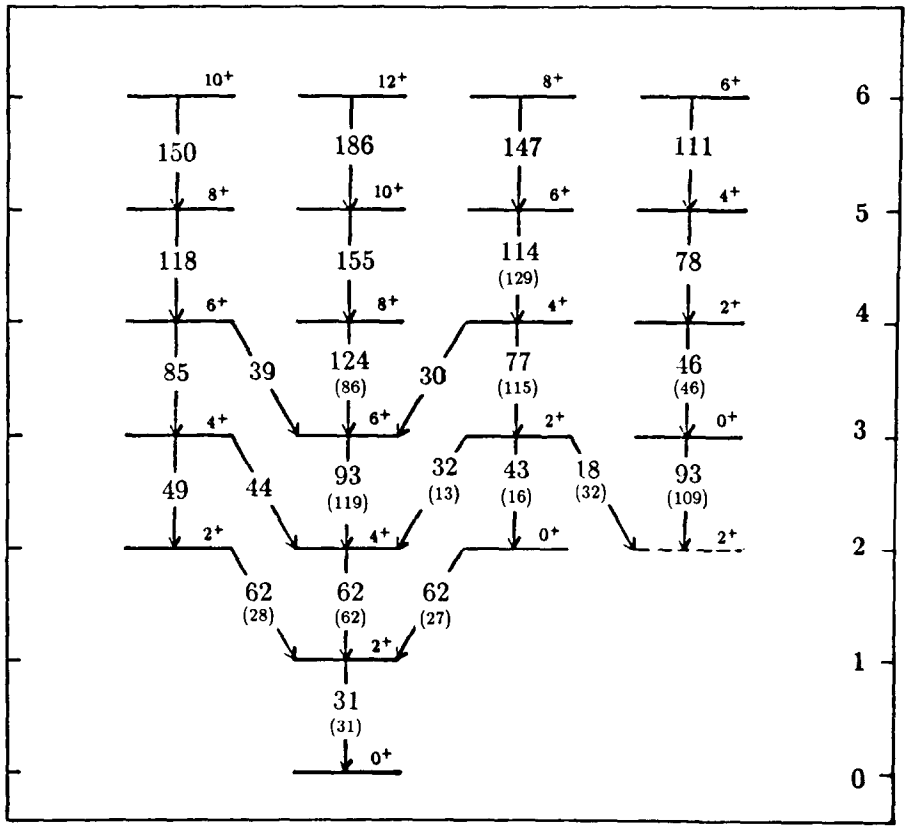

Fig. 14. B(E2) values for some transitions of the harmonic vibrator up to the $N=6$ phonon state, normalised to the experimental value of the $2_1^+ \rightarrow 0_1^+$ transition in ^{114}Cd. The numbers in brackets are the corresponding experimental B(E2) values in W.u.

which are measured in the present experiment, also are in reasonable agreement with these calculations.

In the present study both the quadrupole moments of the 4_1^+ and 6_1^+ states are measured and are found to be negative with rather large magnitudes. They cannot be understood in the harmonic-vibrator model, nor with the inclusion of a small anharmonic term. One possibility is that the quadrupole moments, together with the large energy splitting of the 3- and 4-phonon states discussed above, may be explained as resulting from a potential with large anharmonicity, or that other degrees of freedom are present.

6.2. ROTATIONAL FEATURES IN ^{114}Cd

Although many of the E2 properties of ^{114}Cd are consistent with the vibrational model, there are some features that are in conflict with this model. Some of them were mentioned above. Another example is the E2 transitions from the 0_2^+ and 2_2^+ states to the 1-phonon state, which are only half the value of the vibrational intensity.

This may be interpreted as due to a large anharmonicity, but it may also imply admixture of other configurations. Some of the features of the E2 decay may indicate the presence of deformed states. All $B(E2)$ values measured in the present experiment are shown in the partial level scheme of fig. 15. Strongly enhanced transitions are observed to the 0_4^+, 2_4^+ and 2_5^+ states. Especially, the 0_4^+ and 2_5^+ states are connected with a strong $B(E2)$ transition (although its value is somewhat uncertain, see sect. 4.7). Therefore they may be interpreted as the first two members of a rotational band. Also some of the $B(E2)$ values, discussed above in connection with the vibrational structure, could alternatively be interpreted in terms of rotational band structure.

The sum rule calculation, sect. 5, gives rather large values of the Q^2 parameter for the four 0^+ states. The corresponding β values are 0.17, 0.25, 0.30 and 0.34 for the 0_1^+, 0_2^+, 0_3^+ and 0_4^+ states, respectively. These values are large enough to suggest an interpretation of the level structure in terms of rotational bands. The 2_2^+ state may then be interpreted as the band head of a γ-band. A positive value of 0.92 (5) $e \cdot b$ is measured for its diagonal matrix element, which gives a deformation of $\beta = 0.18$ (1). This is in agreement with the sum rule calculation, which gives a value

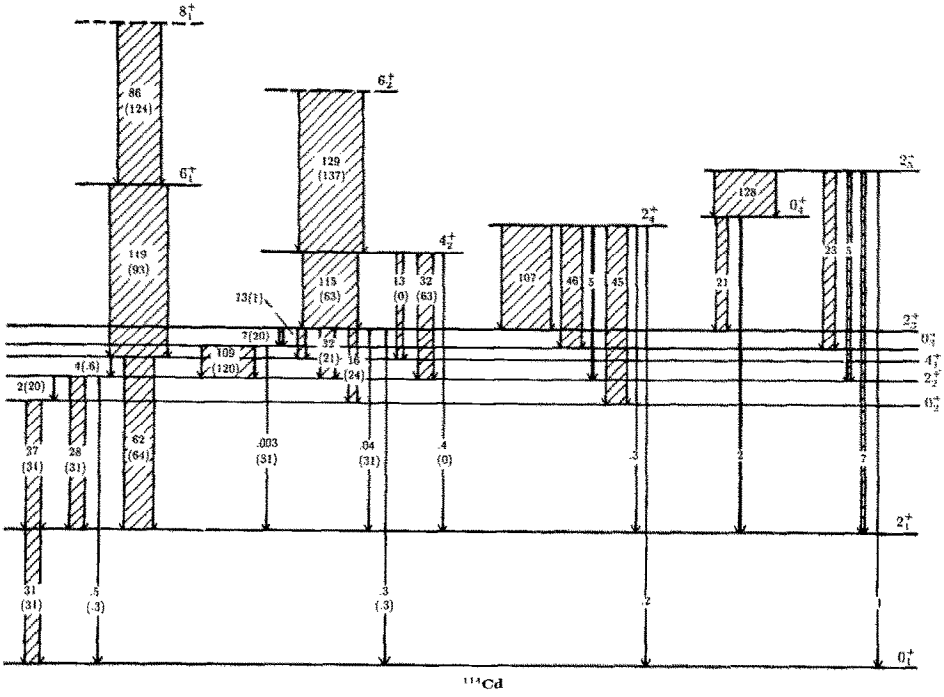

Fig. 15. A partial level scheme of ^{114}Cd. The widths of the arrows are proportional to the experimental $B(E2)\downarrow$. The $B(E2)$ values for transitions coupling to the 0_4^+ state and for the transitions $2_5^+ \to 2_1^+$, $2_4^+ \to 2_2^+$ and $2_4^+ \to 2_3^+$ are uncertain due to the influence from uncertain signs of interference terms and unknown M1 admixtures. The numbers are the experimental and calculated by the simple mixing model (in brackets) $B(E2)\downarrow$ in W.u.

of the expectation value $Q^2 = 0.73\,(12)$, equivalent to $\beta = 0.20\,(2)$. The 4^+ state of the band has not been identified, but may be the 4_3^+ state as discussed in sect. 4.8.

A possible rotational band structure of ^{114}Cd has been discussed previously by several authors. Heyde *et al.* [11]) have suggested that the 0_3^+ and 2_3^+ states are the first two members of a deformed band. This is suggested also in ref. [18]), with the additional proposal that the 4_2^+ state is the third band member. The deformation is supposed to arise from the promotion of 2 protons across the closed $Z = 50$ shell (2p4h excitation), which has been suggested to be the mechanism responsible for the intruder bands observed in the Sn and Te nuclei [1-3]). These calculations are referred to in more detail in sect. 6.3. The promotion of two protons give rise to a second minimum in the potential energy surface on the prolate side, because of the behaviour of the Nilsson orbitals around $Z = 50$ [ref. [39])]. The question of which of the 0^+ states is the intruder state is discussed in ref. [40]), in which it is concluded that the 0_3^+ state is the one having the main part of the intruder configuration in ^{110}Cd and ^{112}Cd, and that in ^{114}Cd the 0_2^+ and 0_3^+ states are fully mixed. The intruder state should have a rather large ratio $B(\mathrm{E2}; 0_3^+ \to 2_2^+)/B(\mathrm{E2}; 0_3^+ \to 2_1^+)$ and the calculation gives a ratio of about 40. However, this does not explain the experimental ratio, which in ^{114}Cd is about 40 000. Further, the suggested mixing is contradicted by the weak $0_3^+ \to 0_2^+$ E0 transition measured in ref. [10]).

The nuclei ^{110}Cd and ^{112}Cd, which are very similar to ^{114}Cd, have been studied by the (^{3}He, n) 2-proton transfer reaction [41]). There it is found that the collective 0_2^+ state and not the hindered 0_3^+ state, is excited. This is surprising if the 0_3^+ state is the suggested 2p4h intruder configuration and is in contradiction with the 0_2^+ state being mainly vibrational. However, on the basis of this it is suggested [42]) that the 0_2^+ state is the deformed intruder band head. In ^{110}Cd [43]), the ground band is observed up to spin 12 and an intruder deformed band, based on the 0_2^+ state, is observed up to spin 10. The behaviour of the decay of the 0^+ states is explained as a quenching effect, where the 2-phonon triplet and the lowest levels of the intruding band are mixed in a similar kind of calculation as in ref. [11]) (see sect. 6.3). It is then possible to modify the calculated $B(\mathrm{E2})$ values in a major way, such that the decay of the suggested 0_3^+ two-quadrupole phonon state is almost completely quenched due to interference.

The possibility that the cadmium nuclei have two minima in their potential energy surface has been discussed by von Bernus *et al.* [44]). According to these authors the 0_3^+ state belongs to an oblate minimum of the potential energy surface, while the 0_1^+ and 0_2^+ states are spherical.

6.3. MIXING CALCULATIONS

The low-lying levels in ^{114}Cd seem to be difficult to interpret in terms of simple models. It appears that both vibrational and rotational modes of motion may play an important role and that they are intimately connected with each other. One may therefore attempt to describe ^{114}Cd in terms of mixing.

We have made an attempt to qualitatively understand the E2 decay properties in terms of a very simple two-state mixing calculation. The 0_3^+ and 2_3^+ states are assumed to be the first two members of a deformed band, which mix with the 0_2^+ and 2_2^+ states of an anharmonic quadrupole vibrator. The enhanced E2 transitions from the 4_2^+ state to the 2_3^+ state and the 6_2^+ state to the 4_2^+ state (see fig. 15) suggest them to be the next two members of that band. The deformation of the band is simply taken from the Q^2 value obtained for the 0_3^+ state in sect. 5, i.e. $\beta = 0.30$, which is equivalent to an intrinsic quadrupole moment of $|Q_0| = 3.8\ e \cdot \mathrm{b}$. The unmixed rotational E2 matrix elements are now easily calculated and given in column 3 of table 3. The anharmonic vibrator E2 matrix elements are calculated by normalising to the $2_1^+ \to 0_1^+$ transition and assuming an anharmonicity of about 2%. The anharmonicity is obtained from the ratio of the two matrix elements, $\langle 2_1 \| M(\mathrm{E2}) \| 0_1 \rangle$ and $\langle 2_2 \| M(\mathrm{E2}) \| 0_1 \rangle$ [ref. [45])], which is the same in ^{114}Cd as in the neighbouring $^{102\text{-}110}$Pd isotopes [9,46]). This is enough to explain e.g. the quadrupole moment of the first excited 2^+ state. The calculated anharmonic values are also given in column 3 of

TABLE 3

Comparison between experimental E2 matrix elements (in $e \cdot \mathrm{b}$) and the mixing calculations of the present paper and of refs. [11,47])

Transition	Experiment	Unmixed	Mixed	Ref. [47])
$0_1^+ \to 2_1^+$	$0.714^{+0.021}_{-0.021}$	0.714 [a])	0.714	0.714
$0_1^+ \to 2_2^+$	$0.091^{+0.003}_{-0.003}$	0.091 [a])	0.064	0.042
$0_1^+ \to 2_3^+$	$0.073^{+0.003}_{-0.002}$	0.00	−0.064	0.018
$0_2^+ \to 2_1^+$	$0.300^{+0.007}_{-0.009}$	0.45 [a])	0.32	0.25
$0_2^+ \to 2_2^+$	$-0.17^{+0.04}_{-0.02}$	0.06 [a])	−0.57	−0.68
$0_2^+ \to 2_3^+$	$0.51^{+0.03}_{-0.03}$	0.00	−0.63	0.73
$0_3^+ \to 2_1^+$	$0.00300^{+0.00045}_{-0.00014}$	0.00	0.32	0.23
$0_3^+ \to 2_2^+$	$0.60^{+0.02}_{-0.02}$	0.00	0.63	0.24
$0_3^+ \to 2_3^+$	$0.33^{+0.06}_{-0.08}$	−1.20	0.57	−0.49
$2_1^+ \to 2_1^+$	$-0.36^{+0.01}_{-0.03}$	−0.27 [a])	−0.27	−0.29
$2_1^+ \to 2_2^+$	$0.684^{+0.021}_{-0.021}$	1.01 [a])	0.72	0.74
$2_1^+ \to 2_3^+$	$0.025^{+0.011}_{-0.005}$	0.00	−0.72	0.48
$2_1^+ \to 4_1^+$	$1.35^{+0.04}_{-0.04}$	1.38 [a])	1.38	1.23
$2_1^+ \to 4_2^+$	$0.11^{+0.01}_{-0.01}$	0.00	0.00	0.16
$2_2^+ \to 2_2^+$	$0.92^{+0.04}_{-0.05}$	0.27 [a])	0.86	−0.41
$2_2^+ \to 2_3^+$	$0.71^{+0.02}_{-0.09}$	0.00	0.59	0.71
$2_2^+ \to 4_1^+$	$-0.35^{+0.07}_{-0.02}$	0.18 [a])	0.13	−0.37
$2_2^+ \to 4_2^+$	$0.97^{+0.17}_{-0.03}$	0.00	1.37	1.17
$2_3^+ \to 2_3^+$	$0.29^{+0.10}_{-0.27}$	1.43	0.86	−0.58
$2_3^+ \to 4_1^+$	$0.46^{+0.06}_{-0.02}$	0.00	−0.13	0.31
$2_3^+ \to 4_2^+$	$1.85^{+0.10}_{-0.06}$	−1.92	1.37	−1.28
$4_1^+ \to 4_1^+$	$-0.95^{+0.04}_{-0.11}$	0.00 [a])	0.00	−0.52
$4_1^+ \to 4_2^+$	$0.61^{+0.08}_{-0.04}$	0.00	0.00	0.38
$4_1^+ \to 6_1^+$	$2.26^{+0.34}_{-0.34}$	2.00 [a])	2.00	1.49
$4_2^+ \to 6_2^+$	$2.35^{+0.35}_{-0.35}$	−2.42	2.42	1.68
$6_1^+ \to 6_1^+$	$-3.49^{+0.87}_{-0.87}$	0.00 [a])	0.00	−1.26
$6_1^+ \to 8_1^+$	$2.19^{+0.33}_{-0.33}$	2.63 [a])	2.63	2.36

[a]) Anharmonic vibrator value assuming an anharmonicity of 2%.

table 3. For a qualitative estimate the two 0^+ states and the two 2^+ states are simply assumed to be fully mixed. The amount of mixing is not critical for a qualitative understanding, and a difference in the mixing of up to 20% will not alter the conclusions drawn. A remarkably good agreement is obtained with this simple calculation as shown in column 4 of table 3. The data are also shown in fig. 15, where the numbers in brackets refer to $B(E2)\downarrow$ in W.u. obtained in the present mixing calculation. As already pointed out the decay of the 2_1^+, 4_1^+, 6_1^+ and 8_1^+ states are well reproduced by the anharmonic vibration. The unmixed rotational $B(E2)$ values reproduce the in-band E2 decays of the suggested intruder band, except for the $2_3^+ \rightarrow 0_3^+$ transition. However, as shown in table 3 and fig. 15, the mixing strongly reduces the unperturbed value to 20 W.u., although it does not fully reproduce the measured value of 7 W.u. The unmixed $B(E2)$ values for the transitions between states of the vibrational configuration and the deformed band members are zero in our simple model, whereas several of the corresponding experimental values are enhanced. The values obtained in the mixing calculation are in qualitative agreement with the enhanced experimental values. In the case of the $0_3^+ \rightarrow 2_2^+$ transition the enhancement is more than a factor of 100, but even this large value is reproduced nicely. The transitions from the 2_3^+ and 4_2^+ states to the 4_1^+ state both are enhanced by a factor of 13, whereas the calculated values are 1 and 0 W.u. However, this can be accounted for by a small admixture between the 4_1^+ and 4_2^+ states. The good agreement obtained with this simple model suggests that mixing is important.

The above result is obtained independently of whether a prolate or an oblate deformation for the intruder band is assumed. However, the prolate assumption will not reproduce the large positive quadrupole moment measured for the 2_2^+ state, nor the positive value of the quadrupole moment of the 2_3^+ state. In the mixing calculation both of these quadrupole moments are consistent only with the assumption of an oblate deformation. It is interesting to note, that the 2p4h excitation, suggested to be responsible for the intruder states, induces a prolate deformation as pointed out in sect. 6.2. Further, the strong hindrance of the transitions from the 0_3^+ and 2_3^+ states to the 1-phonon state cannot be reproduced and will only be reproduced in this simple picture if only weak mixing is assumed.

A more sophisticated mixing calculation has been performed by Heyde *et al.* [11]). They have made detailed calculations using two different approaches, both of which emphasize the importance of the particle-hole excitation across the $Z = 50$ closed proton shell. The first approach treats the quadrupole vibrational configurations in interaction with proton 2p4h excitations, and the second approach is a configuration mixing calculation within the interacting boson model (IBA). In the following we will refer only to the IBA type calculations, since the two approaches give rather similar results.

In the IBA calculation the 2p4h excitations are introduced in an approximate way by allowing the normal neutron-proton IBA hamiltonian ($N_\pi = 1$ and $N_\nu = 8$) to interact with a configuration having an additional proton-hole boson and a proton-particle boson, i.e. $N_\pi = 3$. By choosing the np quadrupole-quadrupole force

strength appropriately it is shown how the 0^+ and 2^+ states of the $N_\pi = 3$ configuration are brought down in energy close to the normal triplet of the $N_\pi = 1$ configuration. The energies of the quintuplet of levels thus can be well reproduced. The 0_2^+ and 0_3^+ states and the 2_2^+ and 2_3^+ states of the two configurations are allowed to mix fully.

The calculated E2 matrix elements are in reasonable overall agreement with the experimental data as shown in table 3. Also the relative signs are fairly well reproduced [47]). The enhanced decay of the 0_3^+ state to the 2_2^+ state is obtained through constructive interference between the large E2 matrix elements obtained in both the normal and the intruder configuration space. The almost forbidden 0_3^+ to 2_1^+ transition (hindered by a factor of more than 300 as compared to the Weisskopf estimate), would then be explained as destructive interference between the two strongly collective E2 amplitudes. However, as seen in table 3, this does not work properly, since $\langle 0_3 \| M(\mathrm{E2}) \| 2_2 \rangle$ is underestimated and both the calculated $\langle 0_3 \| M(\mathrm{E2}) \| 2_1 \rangle$ and $\langle 2_3 \| M(\mathrm{E2}) \| 2_1 \rangle$ matrix elements are enhanced over the Weisskopf estimate.

The model also predicts the diagonal matrix elements. The value of $\langle 2_1 \| M(\mathrm{E2}) \| 2_1 \rangle$ is correctly predicted but the values of $\langle 4_1 \| M(\mathrm{E2}) \| 4_1 \rangle$ and $\langle 6_1 \| M(\mathrm{E2}) \| 6_1 \rangle$ are underestimated. The diagonal $\langle 2_2 \| M(\mathrm{E2}) \| 2_2 \rangle$ and $\langle 2_3 \| M(\mathrm{E2}) \| 2_3 \rangle$ matrix elements are predicted to have negative signs. This is in contradiction with our measured positive values.

It is clear that quadrupole collectivity is a dominant feature of the low-lying spectrum of ^{114}Cd. The measured properties are consistent with coexistence and mixing of both vibrational and rotational like structures which have quadrupole deformations ranging from $\beta = 0.17$ to 0.34. The modules used in the discussion do not fully reproduce the complicated collective behaviour but the discussion illustrates the importance and overall features of the quadrupole collective motion in the low-lying spectrum of ^{114}Cd.

7. Conclusion

Through the present work the knowledge of the E2 matrix in ^{114}Cd has been considerably extended in that about 40 static and transitional E2 moments of low-lying levels have been determined. They include all matrix elements between the close-lying levels within the quintuplet of states. Large negative static quadrupole moments are found for the 4_1^+ and 6_1^+ states and a large positive quadrupole moment for the 2_2^+ state. The experimental data are complete enough to make sum-rule calculations possible for the low-lying low-spin states.

As pointed out earlier, rotational-band-like structures have been found in the neighbouring Sn and Te nuclei, and both ^{104}Ru and ^{110}Pd can be described in terms of a quasi-rotational ground-band, a quasi-rotational γ-band and a quasi-rotational 0^+-band. The band structure of ^{114}Cd is more complicated. The measured properties imply the coexistence of both vibrational and rotational collective bands with deformations ranging over a factor of two. Moreover there are many states in close

proximity with the same angular momentum and the interaction between these states can be expected to be strong.

The low-lying properties can be explained partially in terms of mixing between a vibrational structure and an intruder deformed band, of which the first four members have been suggested. However, there are some serious arguments against this picture. Firstly, the hindered transitions from the 0_3^+ and 2_3^+ states are not reproduced. Low-lying 0^+ states with hindered transitions to the 2_1^+ state are a recurring phenomenon of nuclei in this mass region. If they are to be explained in terms of destructive interference between two large E2 matrix elements, the mixing must be such that the two matrix elements completely cancel each other. That the cancellation would be exactly complete in all these nuclei is unlikely. These states fit much better into a more vibrational structure, as members of the 3-phonon multiplet. Secondly the positive quadrupole moments of the 2_2^+ and 2_3^+ states cannot be understood by means of an intruder band, having a proton 2p4h configuration.

Although the models used in the present paper are too simple to accurately reproduce the observed behaviour, the data favour the low-lying states as being mainly vibrational, involving states up to the 4-phonon multiplet, rather than in terms of mixing between a vibrational structure and an intruder deformed band.

Dr. K. Heyde is greatly acknowledged for providing us with his IBA configuration mixing calculations and for useful comments on the manuscript. The authors wish to thank Dr. Rauno Julin for helpful discussions and comments. The work was supported by the Swedish Natural Science Research Council, the US National Science Foundation and the West German Natural Science Research Council.

References

1) J. Kantele, R. Julin, M. Luontama, A. Passoja, T. Poikolainen, A. Bäcklin and N.G. Jonsson, Z. Phys. **A289** (1979) 157
2) J. Bron, W.H.A. Hesselink, A. Van Poelgeest, J.J.A. Zalmstra, M.J. Uitzinger, H. Verheul, K. Heyde, M. Waroquier, H. Vincx and P. Van Isacker, Nucl. Phys. **A318** (1979) 335
3) T.L. Shaw, V.R. Green, N.J. Stone, J. Rikovska, P.M. Walker, S. Collins, S.A. Hamada, W.D. Hamilton and I.S. Grant, Phys. Lett. **B153** (1985) 221
4) A. Bäcklin, N.G. Jonsson, R. Julin, J. Kantele, M. Luontama, A. Passoja and T. Poikolainen, Nucl. Phys. **A351** (1981) 490
5) N.G. Jonsson, A. Bäcklin, J. Kantele, R. Julin, M. Luontama and A. Passoja, Nucl. Phys. **A371** (1981) 333
6) J. Stachel, N. Kaffrell, E. Grosse, H. Emling, H. Folger, R. Kulessa and D. Schwalm, Nucl. Phys. **A383** (1982) 429
7) J. Stachel, P. Hill, N. Kaffrell, H. Emling, H. Grein, E. Grosse, C. Michel, H.J. Wollersheim, D. Schwalm, S. Brussermann and F.R. May, Nucl. Phys. **A419** (1984) 589
8) J. Srebrny, D. Cline, C.Y. Wu, R.M. Diamond, D. Habs, H. Hubel, H. Korner, U. Smilansky, F.S. Stephens, G.R. Young and C. Baktash, Proc. Int. Conf. on Extreme states in nuclear systems, Rossendorf, ed. R. Arlt and B. Kuhn (1980)
9) L. Hasselgren and D. Cline, Proc. Int. Conf. on Interacting Bose-Fermi systems in nuclei, Erice, ed. F. Iachello (Plenum, New York 1980) p. 59

10) R. Julin, J. Kantele, M. Luontama, A. Passoja, T. Poikolainen, A. Bäcklin and N.G. Jonsson, Z. Phys. **A296** (1980) 315
11) K. Heyde, P. Van Isacker, M. Waroquier, G. Wenes and M. Sambataro, Phys. Rev. **C25** (1982) 3161
12) P.M.S. Lesser, D. Cline, P. Goode and R.N. Horoshko, Nucl. Phys. **A190** (1972) 597
13) M.W. Guidry, P.A. Butler, R. Donangelo, E. Grosse, Y.El Masri, I.Y. Lee, F.S. Stephens, R.M. Diamond, L.L. Riedinger, C.R. Bingham, A.C. Kahler, J.A. Vrba, E.L. Robinson and N.R. Johnson, Phys. Rev. Lett. **40** (1978) 1016
14) N.G. Jonsson, A. Bäcklin and J. Kantele, Nucl. Instr. Meth. **152** (1978) 485
15) D. Cline and B. Kotlinski, Nuclear Structure Research Laboratory, Rochester, annual report (1982–83)
16) J.F. Ziegler, J.P. Biersack and U. Littmark, The stopping and range of ions in solids, ed. J.F. Ziegler (Pergamon, New York, 1985)
17) S. Brussermann, K.P. Lieb and P. Sona, GSI Scientific Report, Darmstadt (1982)
18) A. Mheemeed, K. Schreckenbach, G. Barreau, H.R. Faust, H.G. Börner, R. Brissot, P. Hungerford, H.H. Schmidt, H.J. Scheerer, T. von Egidy, K. Heyde, J.L. Wood, P. Van Isacker, M. Waroquier, G. Wenes and M.L. Stelts, Nucl. Phys. **A412** (1984) 113
19) T. Czosnyka, D. Cline and C.Y. Wu, Bull. Amer. Phys. Soc. **28** (1983) 745
20) B. Fogelberg, A. Bäcklin and J. McDonald, Proc. Top. Conf. on problems of vibrational nuclei, Zagreb 1974, ed. G. Alaga, V. Lopac, V. Paar and L. Sips (1975)
21) J. Lange, K. Kumar and J.H. Hamilton, Rev. Mod. Phys. **54** (1982) 119
22) F.K. McGowan, R.L. Robinson, P.H. Stelson and J.C. Ford, Jr, Nucl. Phys. **66** (1965) 97
23) W.T. Milner, F.K. McGowan, P.H. Stelson, R.L. Robinson and R.O. Sayer, Nucl. Phys. **A129** (1969) 687
24) Z.W. Grabowski and R.L. Robinson, Nucl. Phys. **A206** (1973) 633
25) At. Data Nucl. Data Tables **36** (1987) 1
26) R.D. Larsen, J.A. Thomson, R.G. Kerr, R.P. Scharenberg and W.R. Lutz, Nucl. Phys. **A195** (1972) 119
27) Z. Berant *et al.*, Nucl. Phys. **A196** (1972) 312
28) K. Hosoyama, Y. Torizuka, Y. Kawazoe and H. Ui, Phys. Rev. Lett. **30** (1973) 388
29) K. Gillespie *et al.*, J. of Phys. **G2** (1976) 185
30) M.T. Esat, D.C. Kean, R.H. Spear and A.M. Baxter, Nucl. Phys. **A274** (1976) 237
31) K. Alder and A. Winther, Electromagnetic excitation (North-Holland, Amsterdam, 1982) p. 343
32) R. Brenn, H. Spehl, A. Weckherlin, H.A. Doubt and G. van Middelkoop, Z. Phys. **A281** (1977) 219
33) C.Y. Wu, thesis, Nuclear Structure Research Laboratory Report, Rochester, UR-NSRL-275 (1983)
34) K. Kumar, Phys. Rev. Lett. **28** (1972) 249
35) D. Cline and C. Flaum, Proc. Int. Conf. on Nuclear structure studies using electron scattering and photoreaction, Sendai, ed. K. Shoda and H. Ui, vol. 5 (1972)
36) D. Cline, Nucler Structure Research Laboratory Report, Rochester, UR-NSRL-84 (1974)
37) D. Cline, Ann. Rev. of Nucl. Part. Phys. **36** (1986) 683
38) J. de Boer, J. Stokstad, R.G. Symons and A. Winther, Phys. Rev. Lett. **14** (1965) 546
39) K. Heyde, P. van Isacker, M. Waroquier, J.L. Wood and R.A. Meyer, Phys. Reports **102** (1983) 291
40) A. Aprahamian, D.S. Brenner, R.F. Casten, R.L. Gill, A. Piotrowski and K. Heyde, Phys. Lett. **B140** (1984) 22
41) H.W. Fielding, R.E. Anderson, C.D. Zafiratos, D.A. Lind, F.E. Cecil, H.H. Wieman and W.P. Alford, Nucl. Phys. **A281** (1977) 389
42) R.A. Meyer and L. Peker, Z. Phys. **A283** (1977) 379
43) D. Kusnezov, A. Bruder, V. Ionescu, J. Kern, M. Rast, K. Heyde, P. Van Isacker, J. Moreau, M. Waroquier and R. A. Meyer, Helv. Phys. Acta, to be published
44) L. von Bernus, U. Schneider and W. Greiner, Lett. Nuovo. Cim. **6** (1973) 527
45) G. Alaga, Cargèse Lecture Notes in Physics, 1969
46) M. Luontama, R. Julin, J. Kantele, A. Passoja, W. Trzaska, A. Bäcklin, N.G. Jonsson and L. Westerberg, Z. Phys. **A324** (1986) 317
47) K. Heyde, private communication